LRP 458/92 July 1992

PROPERTIES OF DIFFRACTION GRATINGS USED AS OUTPUT COUPLERS IN A QUASI-OPTICAL GYROTRON

M.Q. Tran, H. Cao, J.Ph. Hogge,
W. Kasparek, T.M. Tran and P.J. Paris

submitted for publication in
Journal of Applied Physics

Properties of diffration gratings used as output couplers in a quasi-optical gyrotron

M. Q. Tran, H. Cao, J. Ph. Hogge, W. Kasparek*, T. M. Tran, P.J. Paris
Centre de Recherches en Physique des Plasmas
Association Suisse-Euratom
Ecole Polytechnique Fédérale de Lausanne
21, Av. des Bains, 1007-Lausanne/Switzerland

* Institut für Plasmaforschung
Universität Stuttgart
Pfaffenwaldring 31, D-7000 Stuttgart 80, Germany

Abstract

The design of a diffration grating used as an output coupler for a Fabry-Pérot resonator is presented. We then consider the problem of determining the distortion and the cross-polarization of the incident Gaussian beam. Different types of gratings, plane with straight or curvilinear grooves and elliptical, have been designed and built. The output pattern from a resonator using such a grating has been measured experimentally. We found that the elliptical grating generates the least distortion and cross-polarization. This result is attributed to the geometry of the grooves and is in excellent agreement with numerical calculations.

I. INTRODUCTION

The preferred high power transmission lines designed for electron cyclotron wave systems in thermonuclear plasma research are HE_{11} waveguides. This mode is selected for its extreme low loss. Moreover the radiation field has a Gaussian pattern and is linearly polarized. The use of a metallic waveguide provides shielding against leakage of the electromagnetic energy and, in a reactor, of neutrons in the event of window failure. In transferring power from the microwave source to the HE_{11} waveguide, a Gaussian beam is required to insure an efficient power coupling which can reach 98%.[1]

In a cylindrical resonator gyrotron, the output of the microwave source can be converted into the desired Gaussian mode by a suitable converter.[2] In a quasi-optical gyrotron (Q.O.G.), the usual methods of output coupling[3,4] do not provide a Gaussian beam. In present Q.O.G. experiments, the energy is extracted from the Fabry-Pérot resonator by diffraction around the mirror edge. It is then either fed into an over-moded waveguide[3] or focused using a Cassegrain telescope mirror configuration.[4] Hot and cold tests indicate that the output pattern is far from Gaussian and thus is thus difficult to propagate the microwave beam without non-negligible losses.

We have recently[5,6] proposed a new output scheme for Q.O.G. where one of the resonator mirrors is replaced by a grating arranged in the -1 order Littrow mount (Fig. 1). In this arrangement, only two diffracted waves are generated: the -1 order which provides the feedback power to the resonator and the zeroth order which provides the output. In preliminary experiments,[5,6] the measured Gaussian content of the output beam was

greater than 90%. These experiments also show that the output beam was not perfectly linearly polarized: about 10% of the total energy is cross-polarized with a non-Gaussian pattern. Both the Gaussian content and the amount of cross-polarization are important in determining the amount of useful power which is coupled into the HE_{11} waveguide. To study the influence of the grating geometry on these two quantities, we have designed two types of gratings: the first is a plane grating with straight or curvilinear grooves and the second has an underlying surface ("the grating support" shown later on figure 3) which is a portion of an ellipsoid of revolution. Both gratings have been built and tested at low power.

We consider in this paper the performance of a resonator using such gratings as output couplers. The main issue to be investigated experimentally and numerically is the determination of the cross-polarization and the distortion of the output beam. The detailed design of the grating is first described in Sec. II.A. The grating is defined by the geometry of its support (e.g. plane or elliptical), the diffraction angle θ, the characteristics of the Fabry-Pérot resonator in which it will be used and the desired efficiency in the zeroth order. In the case of the elliptical grating, one must also define the desired magnification of the resonator beam waist size. Specific design parameters taking into consideration the constraints of a Q.O.G. will also be presented.

We then consider the distortion and cross-polarization of a Gaussian beam incident on the grating. The incident electric $\underline{E}^i$ and magnetic $\underline{B}^i$ fields are decomposed into TE ($\underline{E}$ parallel to the grooves) and TM ($\underline{B}$ parallel to the grooves) modes. These components are reflected by the grating with different complex reflection coefficients R_{TE} and R_{TM} which correspond to the respective diffraction efficiencies in the zeroth order.

The electromagnetic field, far from the grating, is then computed using the vector Green's formalism. The details of the entire calculation is presented in Sec. II.B.

The properties of Q.O. resonators using grating couplers were measured in a low power experiment. We have focused our interest in characterizing the output pattern and dependence of the quality factor on frequency (Sec. III). In the discussion (Sec. IV), we shall compare the experimental results with the numerical predictions deduced from the model presented in Sec. II.B. A comparison of the different types of gratings will also be outlined.

II. THEORY

A. Design of the grating

Let us first recall some properties of a plane grating of period d and of infinite extent. A plane wave of wavelength λ incident on this grating with an angle θ of incidence relative to the normal, is diffracted by the grating into several directions (or diffraction orders) θ_n given by the grating formula:

$$\sin \theta_n = \sin \theta + \frac{n\lambda}{d} \qquad (1)$$

In the -1 order Littrow mounting, we have:

$$2 \sin \theta = \frac{\lambda}{d} \qquad (2)$$

If the condition in Eq. (2) is satisfied, the -1 order diffraction is exactly in the direction of incidence. From Eqs. (1) and (2), one can see that for $\lambda/d < 2/3$ only the n=-1 and the n=0 diffracted waves can exist. In a Fabry-Pérot resonator where such a grating replaces one of the mirrors, the zeroth order (or specular reflection) provides the output power while the -1 order provides the feedback in the resonator. Assuming that the spillover losses around the mirror and the grating are negligible (or equivalently that the Fresnel number of the resonator is large), the zeroth order efficiency (in power) defines the quality factor of such a resonator and can be computed using the electromagnetic theory of gratings.[7] In the high frequency range used in Q.O.G., the grating mirror can be considered as a perfect conductor, in which case, the integral formulation[7] of the problem is the most adapted. Using this formulation, the diffraction efficiencies for the TM polarization (i.e. the wave magnetic field is parallel to the grooves) and the TE polarization (i.e. the wave electric field is parallel to the grooves) can be calculated for an arbitrary groove profile. For Q.O.G., we shall consider only sinusoidal grooves whose relatively smooth surface minimizes the risk of RF breakdown. Under the -1 order Littrow mounting condition, Eq. (2), the efficiency for the -1 order depends only on the angle of incidence θ and the groove depth h normalized to the period d. The efficiency e_{-1} in the -1 order is given in Figs. 2(a) and 2(b) for the TE and TM modes. By energy conservation the zeroth order efficiency e_0 is equal to $(1 - e_{-1})$.

When a plane grating is used in a Fabry-Pérot resonator, the grating conditions of Eqs. (1) and (2) can only be satisfied if the beam waist, where the wavefronts are almost plane, is located on the grating mirror. Otherwise, the grating is not in a -1 order Littrow mounting: the feedback into the resonator cannot occur and no resonant mode is excited. As a consequence, in a Q.O.G. the ohmic heat load on the plane grating is too high

because the incident Poynting flux is too large. To avoid this problem, the grating must be such that it would not perturb the Gaussian TEM_{00} pattern of an equivalent resonator formed by two spherical mirrors designed to accommodate both requirements of an optimum beam waist w_0 for the gyrotron interaction and an allowable heat load.[8] A method to design the grating can be devised by considering again the case of the plane wave incident on a plane grating of infinite extent with straight grooves. In this situation the Littrow condition is satisfied if the extremities of the grooves coincide with the intersection of the grating support and the wavefronts which are separated in phase by $\pi/2$. Assuming that the incident wavefronts can be reconstructed while satisfying the Littrow condition at each point on the grating, this procedure can then be extended to Gaussian wavefronts. Knowing the beam waist w_0, the wavelength λ and the distance $D/2$ between the grating and the beam waist w_0, one can determine the intersection of the phasefronts and the grating support. A plane grating constructed using this method will give rise to a diverging beam at the output. With an elliptical surface, the output beam is focused to a waist size optimum for the coupling into an HE_{11} waveguide.

This procedure implies that the groove spacing d is no longer constant over the grating surface, but is defined as

$$d(x,y,z) = \frac{\lambda}{2\,\sin\theta(x,y,z)} \tag{3}$$

where $\theta(x,y,z)$ is the local angle of incidence equal to the angle between the normal to the grating surface and the normal to the wavefronts at the point (x,y,z). To assume constant efficiency, the groove depth h(x,y,z) also has to be adapted so that the point $(\theta(x,y,z), h(x,y,z)/d(x,y,z))$ remains on an iso-efficiency line of Fig. 2.

Mathematically, the sinusoidal profile is defined by the following procedure. The electric field E(x,y,z,t) of a linearly polarized Gaussian beam is given by:

$$E(x,y,z,t) = E_0 \frac{w_0}{w(z)} \exp\{-i\varphi(x,y,z)\} \exp\left\{-\frac{x^2+y^2}{w^2(z)}\right\} \exp(-i\omega t) \qquad (4)$$

where w_0 is the resonator beam waist size and w the wave frequency. The spot size w(z), the radius of curvature of the wavefronts R(z), the Rayleigh length z_R, and the phase angle $\varphi(x,y,z)$ are defined respectively as :

$$w(z) = w_0 \left(1 + \frac{z^2}{z_R^2}\right)^{1/2} \qquad (5)$$

$$R(z) = z\left(1 + \frac{z_R^2}{z^2}\right) \qquad (6)$$

$$z_R = \frac{\pi w_0^2}{\lambda} \qquad (7)$$

$$\varphi(x,y,z) = kz + \frac{k(x^2+y^2)}{2R(z)} - \tan^{-1}\left(\frac{z}{z_R}\right) \qquad (8)$$

where k is the wavenumer.

In a resonator characterized by the distance D between the mirrors and the resonator parameter g ($g = 1-(D/R_c)$, where R_c is the radius of curvature of the spherical mirrors), w_0 and z_R are given by [9]:

$$w_o = \left(\frac{D\lambda}{2\pi}\right)^{1/2}\left(\frac{1+g}{1-g}\right)^{1/4} \tag{9}$$

$$z_R = \frac{D}{2}\left(\frac{1+g}{1-g}\right)^{1/2} \tag{10}$$

As mentioned before, the positions of the grooves are deduced from the intersections of the grating support (ellipsoid or plane) and the wavefronts ($\varphi(x,y,z)$ = constant). The intersections with the wavefronts $\varphi(x,y,z) = n\pi$ ($n=1,2,...$) arbitrarily define the highest point of each groove. For a given point A(x,y,z) on the grating support, the vector $\underline{p}(x,y,z)$ from A(x,y,z) to the corresponding grating profile point G(x,y,z) (see Fig. 3) then varies linearly with the cosine of the phase $\varphi(x,y,z)$ at the point A(x,y,z):

$$\underline{p}(x,y,z) = \frac{h(x,y,z)}{2}\,[\cos(2\varphi(x,y,z)) - 1]\,\underline{n}(x,y,z) \tag{11}$$

where $\underline{n}(x,y,z)$ is the outward normal to the grating support at the point A(x,y,z).

In summary, the design of the grating coupler for the Q.O.G. can be performed in three steps:

1) Choose the parameters of the equivalent Fabry-Pérot resonator which meet the requirements of the Q.O. gyrotron.[8] This determines the wavefronts ($\varphi(x,y,z)$ = constant) at the location of the grating.

2) Knowing the desired efficiency in the zeroth order and the operating mode (TE or TM), determine the angle of incidence θ and the groove depth h/d, by using the theory of plane gratings[7] or Figs. 2(a) and 2(b).

3) Calculate the groove profile using the procedure described above.

Let us now discuss in detail the points 1 and 2 of the above prescription. Except for the plane grating with straight grooves described in Sec. IIIA, the resonator and grating parameters were chosen to fit the requirements of actual Q.O.G. The two main parameters of the resonator of a Q.O.G. are the beam waist and the resonator g-factor. The beam waist w_0 (Eq. 9) is the characterisic length over which the electron beam of the Q.O.G. interacts with the electromagnetic fields. The power extraction is optimal for $kw_0 = 15$ to 20.[8] The heat load on the mirrors is proportional to (1+g). The maximum allowable peak heat load for high power gyrotrons is $\rho_{ohmmax} = 1.5$ kW/cm^2.[10,11] Since the heat load on the grating has not yet been computed, the resonator parameters are determined so that ρ_{ohmmax} remains well below this limit, typically $\rho_{ohmmax} \leq 0.5$ kW/cm^2 and g is in the range of -0.5 to -0.8. g and D completely define the resonator and the wavefronts $\varphi(x,y,z)$.

The determination of the angle of incidence and the groove depth h/d is based on the desired two-way loss T of the resonator (T = 1-10%) and the expected operating mode of the Q.O.G. First, since the electric field in a Q.O.G. resonator is quite high, typically 1-10 MV/m, a sinusoidal profile is selected to maximize the radius of curvature of the groove in order to reduce the risk of RF breakdown.

To determine the angle of incidence θ, we must consider whether the Q.O.G. will operate at the first harmonic of the electron cyclotron frequency Ω ($\omega = \Omega$) or its second harmonic ($\omega = 2\,\Omega$). In the first case, we want to suppress the parasitic oscillation at the second harmonic.[12] In the

second case, there should not be any resonant mode of the resonator at the fundamental $\omega = \Omega$.

Under the -1 Littrow mount condition, the grating is automatically in the -2 Littrow mount for the parasitic oscillation in the second harmonic. Figures 4(a) and 4(b) represent the -2^{nd} order efficiency for TE and TM modes at the second harmonic. They clearly show that one can find parameter domains (θ and h/d) which minimize the feedback (i.e. an efficiency in the -2^{nd} order less than 5%) for the second harmonic $\omega = 2\,\Omega$, for a given efficiency at the fundamental $\omega = \Omega$. Resonance at $\omega = 2\,\Omega$ can thus be avoided.

On the other hand, for a grating designed to operate in the -1 Littrow mount at $\omega = 2\Omega$, the -1 Littrow oscillation is not satisfied at the fundamental $\omega = \Omega$: the feedback into the resonator will not be provided for the fundamental. In such conditions, the resonator exhibits resonances at $\omega = 2\Omega$ and not at $\omega = \Omega$. For the same reason, it will not resonate at $\omega = 3\Omega$. Should parasitic oscillations at the fourth harmonic be excited (which is unlikely for typical gyrotron electron beams), their suppression can be performed using the method previously described.

The ability to select the resonance at $\omega = \Omega$ or at $\omega = 2\,\Omega$ is an advantage of the grating resonator over conventional resonators for which the quality factor Q is a monotonically increasing function of frequency.

Finally, for practical reasons the TM polarization was preferred for the tests because the -1 order efficiency is relatively insensitive to the angle of incidence in the domain of interest (h/d ~0.3, θ=25° to 45°). This is a simplification for the manufacture of the gratings because the ratio

h(x,y,z)/d(x,y,z) can be kept constant over the entire surface of the grating (see Fig. 2(a)).

If the output beam is coupled to an HE_{11} waveguide, it is necessary that the field pattern at the input of the guide corresponds to the beam waist of the Gaussian beam with a waist size w_1 equal to 0.645 times the guide radius a.[1] In the case of a plane grating, matching optics are necessary since the output beam is diverging. They could be avoided if one uses an elliptical grating. The parameters of the ellipsoidal support is then designed to achieve the required magnification w_1/w_0.

The results of the application of this method are presented in Fig. 5 for a plane grating and in Fig. 6 for a grating with an elliptical support. It is important to note that the grooves are much more curved in the first case than in the second.

B. Diffraction of a Gaussian beam by a grating

We now wish to compute the distortion and cross-polarization of the output beam of the resonator described in Sec. II. A: We assume that the resonator modes are not affected by the grating. It was verified experimentally that a TEM_{oo} mode is still Gaussian. Therefore, the problem reduces to the determination of the distortion and cross-polarization of a Gaussian beam diffracted by the grating. In SI units, the electric and magnetic fields of the incident wave are respectively $\underline{E}^i$ and $\underline{B}^i$:[13]

$$\underline{B}^i = \underline{\nabla} \times \underline{A} \tag{12}$$

$$\underline{E}^i = \frac{1}{\varepsilon_o \mu_o} \frac{i}{\omega} \underline{\nabla} \times \underline{B}^i \tag{13}$$

where the potential vector $\underline{A}(x,y,z,t)$ is:

$$\underline{A}(x,y,z,t) = A_o U(x,y,z,t)\, \underline{e}_x \qquad (14)$$

$$U(x,y,z,t) = \frac{w_o}{w(z)} \exp\left\{i\left[kz - \tan^{-1}\left(\frac{z}{z_R}\right) - (x^2+y^2)\left[\frac{1}{w^2(z)} - \frac{ik}{2R(z)}\right]\right]\right\}\exp(-i\omega t) \qquad (15)$$

where $\underline{e}_x$ is the unit vector in the x direction (Fig. 1), A_o an arbitrary constant.

Since the grooves are not straight (Figs. 5 and 6), at any point on the grating G(x,y,z) the incident field is neither a TE nor a TM mode. As in usual waveguide theory, we decompose the incident field into TE and TM modes. Let us define at each point on the grating a set of orthogonal unit vectors ($\underline{e}_a$, $\underline{e}_b$, $\underline{e}_c$) (Fig. 7) where $\underline{e}_c$ is perpendicular to the grating and $\underline{e}_a$ and $\underline{e}_b$ are in the plane tangent to the grating support with $\underline{e}_b$ tangent to the groove. $\underline{e}_a$, $\underline{e}_b$ and $\underline{e}_c$ are, of course, dependent on the position (x,y,z) on the grating. Furthermore we assume that, locally, the incident wave can be considered as a linearly polarized plane wave with the incident wavevector $\underline{k}^i$ normal to the wavefront. $\underline{E}^i(x,y,z)$ and $\underline{B}^i(x,y,z)$ are given by :

$$\underline{E}^i = E_a \underline{e}_a + E_b \underline{e}_b + E_c \underline{e}_c \qquad (16$$

$$\underline{B}^i = B_a \underline{e}_a + B_b \underline{e}_b + B_c \underline{e}_c \qquad (17)$$

By definition, $\underline{E}_i = E_b\underline{e}_b$ and $B_b = 0$ for the TE mode and $\underline{B}^i = B_b\underline{e}_b$ and $E_b = 0$ for the TM mode. B_a and B_c (resp. E_a and E_c) are straightforwardly deduced from E_b (resp. B_b) using the assumption of a plane wave (i.e. $-\omega\underline{E}^i$

$= c^2(\underline{k} \times \underline{B}^i))$ in the TE (TM) mode. The incident wave vector $\underline{k}^i$ is perpendicular to the groove direction at all points on the grating ($\underline{k} \cdot \underline{e}_b < 5 \cdot 10^{-4}$ from the numerical calculations performed with typical gratings suitable for Q.O.G.) and therefore $\underline{k}^i$ is equal to $k_a \underline{e}_a + k_c \underline{e}_c$. This last consideration implies that effects due to the conical diffraction are negligible[7] and the simple electromagnetic theory of diffraction is applicable. Let R_{TE} and R_{TM} be the complex efficiency coefficients in the zeroth order mode. Though the angle of incidence θ only varies by less than 5^o over the grating surface, we have included the corresponding variation of R_{TE} and R_{TM} with Θ in the formalism. For the values of θ and h/d corresponding to a typical grating (Table I), R_{TE} and R_{TM} are quite different and, therefore, the "reflected" fields will suffer from cross-polarization. The corresponding reflected reflected electric (magnetic) field for the TE (TM) mode is $R_{TE}\, E_b \underline{e}_b$ ($R\ TM\ B_b \underline{e}_b$). The remaining components of the reflected fields $\underline{E}^d(x,y,z)$ and $\underline{B}^d(x,y,z)$ for both the TE and TM modes are obtained from Maxwell's equations using $\underline{k}^d = k_a \underline{e}_a - k_c \underline{e}_c$:

$$\underline{E}^d = - R_{TM}\, E_a \underline{e}_a + R_{TE}\, E_b \underline{e}_b + R_{TM}\, E_c \underline{e}_c \qquad (18)$$

$$\underline{B}^d = - R_{TE}\, B_a \underline{e}_a + R_{TM}\, B_b \underline{e}_b + R_{TE}\, E_c \underline{e}_c \qquad (19)$$

The fields $\underline{E}^d$ and $\underline{B}^d$ are thus defined at every point on the grating surface. The diffracted fields $\underline{E}^o$ and $\underline{B}^o$ at a point P away from the grating are obtained from $\underline{E}^d$ and $\underline{B}^d$ using electromagnetic theory of diffraction.[14] A vector formalism is necessary to consider issues concerning cross-polarization of the fields away from the grating surface. Since we shall be mainly concerned with the pattern in the zeroth order, it is more convenient to express $\underline{E}^o$ and $\underline{B}^o$ in the frame (x',y',z') (Fig. 1). O'z' is the axis of the beam diffracted in zeroth order. The two frames (x,y,z) and (x',y',z') are related by

a rotation of twice the angle of incidence θ. In the rest of the paper, prime quantities will refer to the (x',y',z') frame. From the Stratton and Chu formulae,[14] we obtain the field $\underline{E}^o$ and $\underline{B}^o$ at the point of observation (x',y',z') from the field $\underline{E}^d$ and $\underline{B}^d$ computed at every point of the grating surface (x'g,y'g,z'g).

$$\underline{E}^0(x',y',z') = -\frac{1}{\varepsilon_0\mu_0}\frac{1}{4\pi i\omega}\int_\Gamma \underline{\nabla}\Psi(\underline{B}^d \bullet d\underline{l})$$

$$-\frac{1}{4\pi}\int_{\Sigma_g}\left[i\omega[\underline{n}\times\underline{B}^d]\Psi + (\underline{n}\times\underline{E}^d)\times\underline{\nabla}\Psi + (\underline{n}\bullet\underline{E}^d)\,\underline{\nabla}\Psi\right]dS \qquad (20)$$

$$\underline{B}^o(\underline{x}',y',z') = \frac{1}{4\pi i\omega}\int_\Gamma \underline{\nabla}\Psi(\underline{E}^d \bullet d\underline{l})$$

$$+\frac{1}{4\pi}\int_{\Sigma_g}\left[i\omega\,\varepsilon_0\mu_0\,(\underline{n}\times\underline{E}_d)\Psi - (\underline{n}\times\underline{B}^d)\times\underline{\nabla}\Psi - (\underline{n}\bullet\underline{B}^d)\,\underline{\nabla}\Psi\right]dS \qquad (21)$$

Γ is the line contour circling the grating edge and Σ_g the grating surface. Ψ is the three dimensional Green's function:

$$\Psi = \frac{\exp\{ikr\}}{r} \qquad (22)$$

The distance r is measured from the element (x'_g, y'_g, z'_g) on the grating to the point of observation P (x', y',z'). $\underline{n}$ is the outward normal from the surface Σ_g.

Since the incident electric field is mainly linearly polarized along Ox, the zeroth order diffracted beam also has its electric field along O'x'. We de-

fine the O'x' direction as the correct polarization direction for the diffracted beam, the cross-polarization being in the O'y' direction. The Gaussian content in power, C^2, of the diffracted beam and the amount of cross-polarization XP are defined as:

$$C^2 = \frac{\left[\int_{\Sigma_0} dx'dy' \sqrt{S_{x'}} \exp\left\{-\frac{x'^2 + y'^2}{w'^2}\right\}\right]^2}{\left[\int_{\Sigma_0} dx'dy' S_{x'}\right] \left[\int_{\Sigma_0} dx' dy' \exp\left\{-\frac{2(x'^2 + y'^2)}{w'^2}\right\}\right]} \tag{23}$$

$$XP = \frac{\int_{\Sigma_0} dx'dy' S_{y'}}{\int_{\Sigma_0} dx'dy' S_{x'} + \int_{\Sigma_0} dx'dy' S_{y'}} \tag{24}$$

$S_{x'}$ and $S_{y'}$ are :

$$S_{x'} = \frac{\left|Re\left[E^o_{x'} \bullet B^{o*}_{y'}\right]\right|}{\mu_0} \tag{25}$$

$$S_{y'} = \frac{\left|Re\left[E^o_{y'} \bullet B^{o*}_{x'}\right]\right|}{\mu_0} \tag{26}$$

which are the absolute values of the two contributions to the z' component of the Poynting vector. The surface Σ_0 is the area over which the field pattern is computed. Σ_0 is chosen to be large enough compared to the corresponding beam-waist size so that the fields are small at its boundary. Equation (23) gives a slightly overestimated value since the phase of the electric field is not taken into account. Nevertheless, when the integration is made near the focal point, where the phase of a Gaussian beam is con-

stant in the plane perpendicular to the direction of propagation, and when the pattern is close to a Gaussian, this estimation is quite good.

In summary by evaluating the "reflected" fields $\underline{E}^d$, and $\underline{B}^d$, Eqs. (18) and (19), on the grating surface and then the fields $\underline{E}^o$ and $\underline{B}^o$, Eqs. (20) and (21), at the observation point, one can determine the Gaussian content C^2 and the cross-polarization content XP for any grating. The evaluation of $\underline{E}^d$ and $\underline{B}^d$ involves lengthy computations which take into account the exact geometry of the grooves. They have been performed for the two types of gratings under investigation: the plane grating and the elliptical grating. The coefficients C^2 and XP have been evaluated at different z' for these two designs.

The code was bench-marked by replacing the grating with a perfectly reflecting plane mirror. In the present formalism, this is equivalent to using $R_{TE} = 1$ and $R_{TM} = -1$. We have verified numerically that the reflected beam is Gaussian and fits exactly the pattern deduced from Eqs. (12) to (15). Energy conservation in the reflected beam was also checked .

III. COLD TEST RESULTS

A. Experimental set-up

The cold test experimental set-up is shown on Fig. 1. The RF source was a carcinotron ($P_{RF} \leq 1$ W, $f_{RF} = 90$ to 120 GHz). The resonator was composed of a spherical metallic mirror and a diffraction grating placed in Littrow mount. A WR-10 rectangular waveguide was used to couple the RF power into the cavity. The resonator was excited through a small hole

(ϕ = 1.1 mm) drilled in the center of the spherical mirror. The dimensions of the spherical mirror and the grating correspond to four spot-sizes w_m, the spot-size defined as the distance at which the electric field decreases by a factor of 1/e, or, equivalently, to a Fresnel number of 2. With this design, the spillover losses are small (< 0.1%): all energy lost by the resonator is concentrated in the zeroth order of the grating, and the distortion induced by the finite size of the grating is negligible. An experiment with different grating sizes (L/w_m = 7,6,5,4 where L is the grating size) has confirmed the latter assertion. Neglecting the ohmic and spillover losses, the zeroth order grating efficiency e_0 is then directly related to the cavity quality factor Q and the two-way loss T [15] by:

$$e_0 \cong T \cong \frac{4\pi D}{Q\lambda} = \frac{4\pi D}{\lambda}\,\frac{\delta\omega}{\omega}. \qquad (27)$$

The full width at half maxium $\delta\omega$ of the resonance curve gives the two way loss T.

The output pattern of the microwave beam was recorded by a Schottky diode mounted on an XY table, allowing scans over a 10x10 cm^2 area. Measurements at larger distances were performed by placing the detector on a circular optical rail. The dynamic range of detection was about 30 dB.

The Gaussian content in power, C^2, and the cross-polarization content, XP, of the diffracted beam were computed from formulae (23) and (24). w' was taken as the theoretical value of the beam waist. No adjustment was performed to optimize the value of C^2. The detector antenna was a standard WR-10 rectangular horn, sensitive to one electric field polarization direction (either x' or y') of the electric field only. A rotation of

90° of the horn was performed to record the cross-polarized signal $S_{y'}$. The crosstalk of the system (i.e. the ratio $S_{y'}/S_{x'}$ corresponding to the case of an electric field which is linearly polarized in the x' direction) was measured using a Gaussian horn as a source of the electromagnetic wave, The crosstalk was measured to be less than the values measured with the grating (-20 dB to -13 dB).

The output beam was also coupled into a 2 m HE_{11} corrugated waveguide. The guide diameter was 2.5 inches and it was made of copper with an NiP coating to damp higher order modes. The transmission bandwidth of the guide extended from 90 GHz to 190 GHz.

Three sets of experiments were performed, using a plane grating with periodic straight grooves, a plane grating with curvilinear grooves and finally an ellipsoidal grating with curvilinear grooves. The parameters of the different resonators are summarized in Table I. With the exception of the plane grating with straigth grooves, the resonator and grating parameters were chosen to meet the requirements of actual Q.O.G.

In the millimeter wavelength range, the machining of the gratings is difficult. In order to simplify the manufacture, a point source approximation was performed. In the case of a plane grating, the curvilinear grooves thus become concentric circles with varying spacing d and depth h. A computer-controlled lathe was used for the machining. For the ellipsoidal gratings a lathe or a milling could also be used since, under the point source approximation, the grooves are circles centered on the main axis of the ellipsoid. Note that the validity of the point source approximation requires that the distance D between the grating and the spherical mirror of the resonator is larger than four times the Rayleigh length z_R (Eq. 10).

B. Plane periodic grating with straight grooves

To verify the validity of the electromagnetic theory of gratings in the case of a finite-extent grating, we considered first the plane periodic grating as a coupler for a resonator. As mentioned in Sec. II, the resonator beam waist w_0 is located on the grating and hence w_m and w_0 are equal (first column of Table I).

The squares on Fig. 8 represent the two-way loss T of the TEM_{00} modes as a function of frequency. The incidence angle was optimized for each frequency in order to satisfy the Littrow condition. A good agreement was found between theory (solid line) and experiment. To study the influence of the finite size of the incident wave, we have changed the radius of curvature R_c of the spherical mirror and the mirror spacing D to reduce the spot-size on the grating. The triangles on Fig. 8 then represent the two-way loss T of the TEM_{00} modes in the case where kw_0 is decreased from 35.2 to 18.9 by changing D from 80.5 mm to 180 mm and R_c from 1160 mm to 234 mm. In these conditions, the spot-size on the grating is too small compared to the grating periodicity d and the assumption of plane waves of infinite extent fails. The zeroth order efficiency differs slightly from the theoretical prediction. It has been shown by Wirgin and Deleuil[17] that a plane grating can be considered as infinite when the number of grooves is larger than about 12. In our experiment, if we use $2\,w_m$ as the extent of the wave, the corresponding number of grooves drops from about 14 to 7, in agreement with the result of Wirgin and Deleuil.[16] However, the inaccuracy in the determination of the zeroth order two-way loss is small even at small values of w_m. All of the gratings which have been tested had kw_m larger than 30 (Table I).

An angular scan of the output was made at 120 cm from the grating. As shown on Fig. 9, only one maximum was detected along the diffraction angle. No higher diffraction order was observed. The two-dimensional radiation output pattern (Fig. 10) was measured. The experimental curve was fitted with a Gaussian: the Gaussian content C^2 is larger than 99%. This estimate, however, should be considered as an upper limit of C^2, since we were only able to measure the pattern over a dynamic range of 5 dB. This limitation was due to the large spot size of the diverging beam at the observation point. The cross-polarization content was negligible.

C. Plane grating with curvilinear grooves

Following the principle described in Sec. II, we designed a plane grating keeping the beam waist at the center of the resonator. The Littrow condition was satisfied along one line. The geometry of the grating can be approximated by circular concentric grooves (Figs. 5). The diffracted beam was divergent and an elliptical mirror was used to focus the beam into an HE_{11} waveguide. The parameters of two such resonators are given in Table I.

Let us consider first the performance of resonator #1 (second column of Table I). Figure 11(a) shows the pattern of a TEM_{00} mode measured at the input of an HE_{11} waveguide. The separation between the contours of equal intensity is 3 dB. A comparison to the ideal Gaussian beam at this point (Fig. 11(b)) shows that the agreement is very good, and the coupling factor C^2 is higher than 98%. Figure 12 is a contour plot of the cross-polarized signal. About 10% to 15% of the power was measured to be cross-polarized. Taking into account the depolarization losses, the coupling

factor C^2, and the coupling factor[1] of the ideal Gaussian beam to the HE_{11} mode, the overall efficiency was estimated to be 83%.

Figures 13(a) and 13(b) represent the contour plots of the field radiated by the corrugated waveguide after 2 m of propagation, and of the ideal radiated Gaussian beam. The measurement was taken 1 m from the waveguide aperture. Here again the agreement between theory and experiment is very good and the Gaussian content C^2 in the original polarization is 99%.

Resonator #2 (third column of Table I) was designed to fit into the cold cross-bore of a compact Q.O.G.:[17] the angle of incidence was chosen to avoid the excitation region of the second harmonic and the resonator parameters were selected so that the whole system including the matching optics (an elliptic mirror) could be inserted into the superconducting magnet. The measured Gaussian content C^2 and the cross-polarization XP are 90% and 7% respectively: the computed coupling efficiency to an HE_{11} waveguide is therefore about 82% = .90 × .93. We have also verified experimentally that there was no resonance at the second harmonic (Frequency around 180 GHz). Great care was exercized to insure that this observation did not result from a poor coupling from the source to the resonator at 180 GHz.

D. Ellipsoidal grating

Using the design principles outlined in Sec. II, we have found that if the grating support is ellipsoidal, the grooves are only slightly curved compared to those of the plane gratings (Figs. 5 and 6), and thus depolarization associated with the TE-TM incidence should be reduced (cf. Sec. IV).

Moreover, the need for matching optics can be avoided. To simplify the machining of the grating, the Littrow condition is only met on one line perpendicular to the grooves.

The parameters of the ellipsoid were chosen such that the diffracted beam has the optimal beam waist for coupling into the HE_{11} corrugated waveguide: the magnification w_1/w_o was 2.19 (Table I). The distances R_1 and R_2 from the focal points of the ellipsoid to the point of incidence correspond respectively to the radii of curvature of the resonator mode and of the diffracted beam at the point of incidence on the grating in order to minimize the coma aberration.[18]

Figure 14(a) shows the output pattern of the grating resonator for a TEM_{00} mode at 92.4 GHz, measured at the focal point. The lines of equal intensity are separated by 2 dB. The Gaussian content C^2 is 98.6%. The -8.68 dB line correponds to a waist kw_1=39.67, which is very close to the ideal value kw_1 = 39.48. The cross-polarized pattern is shown in Fig. 15(a), where the lines are separated by 1 dB. The amount of cross-polarized signal XP is 2.9%. Taking into account the coupling factor to the HE_{11} mode of a corrugated waveguide,[1] the global coupling factor from the output into an HE_{11} waveguide is estimated to be 94%.

In the framework of Q.O. gyrotron development an important issue is the mode competition. Figure 16 represents the two-way loss T of the TEM_{00} modes as a function of the frequency for two fixed angles of incidence θ, θ = 28° and 27.5° respectively. For a given angle of incidence θ, only a few modes have the designed two-way loss T. For the other adjacent modes, the Littrow condition is not as well satisfied as for the central one and, even though they were still resonant modes, the resonator behaved as

if it were misaligned. A slight tilt of the grating had the effect of tuning the frequency of the mode which had the highest quality factor Q. The minimum two-way loss for the curves of Fig. 16 are shown to be unequal, in agreement with theory (Fig. 2(a)). This is an important difference between this type of resonator and conventional resonators for which the quality factor of the longitudinal modes are almost constant within the instability bandwidth (about 3%) of the gyrotron instability. It can be expected that the mode competition in a Q.O.G. would be strongly affected by the frequency dependence of the resonator two-way loss T (or equivalently the quality factor Q) of the longitudinal modes.

Transverse modes could also be excited in the resonator. They did not possess a cylindrical symmetry but rather a rectangular one due to the grating shape and the groove distribution on the grating. The observed pattern was similar to the one of the TEM_{02} mode. The two-way loss T of these high order transverse modes were larger than that of the TEM_{00} mode. The increase of T is due to the increase in the diffractive loss of higher order modes for a given Fresnel number. The diffractive properties of the grating do not depend on the incident TEM_{mn} mode, since the expression for the radius of curvature R of the wavefront is the same for all modes.

IV. DISCUSSION

A comparison of the plane with curvilinear grooves and the elliptical grating shows that the latter exhibits the best performance: the Gaussian content C^2 is greater and the amount of cross-polarization XP is smaller. Table II gives a summary of the results for the two types of gratings which

have comparable kw_0 and g-parameters (third and fourth columns of Table I). Preference was therefore given to the elliptical grating for the hot test which is under preparation.

For both types of gratings designed relevant to the Q.O.G., the power in the cross-polarization cannot be neglected. XP was about 6% to 12% for the plane grating with curvilinear grooves and 3% for the ellipsoidal grating. In the latter case, both the distortion and cross-polarization generated by a smooth ellipsoidal support have been estimated and are negligible. Their magnitudes can be estimated at first order in $(w_m/f)^2$ where w_m is the spot size on the grating support and f is the focal length of the ellipsoid:[18]

$$\text{Distortion loss} = (1- C^2) = \frac{1}{8}\left(\frac{w_m}{f}\right)^2 \tan^2\alpha \qquad (28)$$

$$\text{Cross-polarization loss} = XP = \left(\frac{w_m}{f}\right)^2 \tan^2\alpha \qquad (29)$$

where α is the angle of incidence on the ellipsoid. In our case α is equal to θ. The focal length f of the ellipsoid is defined as:

$$\frac{1}{f} = \frac{1}{R_1} + \frac{1}{R_2} \qquad (30)$$

where R_1 and R_2 are the distances from the foci to the point of incidence.

In the present case, w_m/f is 0.130 and the losses due to distortion and cross-polarization are respectively 0.12% and 0.06%. They are negligible compared to the measured values of $(1 - C^2)$ = 2% and XP = 6%.

The observed cross-polarization is due to the non-pure TE and TM incidence as well as to the variation $\Delta\theta$ of the angle of incidence on the grating was 3° (1°) for the plane ellipsoidal one grating. To verify these assumptions, we computed the cross-polarization and distortion of a Gaussian beam incident on a grating using the theory outlined in Sec. IIB. The comparison was performed for the two gratings of the third and fourth columns of Table I.

The computed correct polarization power contour plots are given for the elliptical and plane gratings in Figs. 14(b) and 17(b). For the elliptical grating the distance z' = 230 mm corresponds to the minimum waist for the zeroth order diffracted beam. In the case of the plane grating, the patterns were computed at the same location (z' = 110 mm) where the measurements were performed. The lines are equi-power lines separated by -2 dB. The incident Gaussian beam is only weakly distorted in the case of an elliptical grating: the Gaussian content C^2 at the beam waist is as high as 98%. Note that C^2 is computed using a value of w equal to the theoretically predicted value and we did not optimize C^2 by varying w. On the contrary, the plane grating introduces much larger distortion on the zeroth order diffracted beam (C^2 ~90%). Similarly, the computed cross-polarization content XP (Figs. 15(b) and 18(b)) is larger in the case of a plane grating than in the case of the elliptical grating. It is interesting to point out that the cross-polarization contour corresponds to a TEM_{01} mode (azimuthally asymmetric mode). For the experimentally-measured case of the plane grating (Fig. 18(a), the diffracted beam is divergent and the amount of power was insufficent to perform a precise measurement of the cross polarization content XP. To get an estimate of XP, we added an elliptical mirror to focus the beam into a HE_{11} waveguide, thus increasing the power level. The distortion of the pattern in Fig. 17 is due to the very strong

curvature of the grooves on the corresponding side of the plane grating. In Table II, we reported the measured and computed values of C^2 and XP. An excellent agreement was found between theory and experiment.

An elliptical grating yields both less distortion and less cross-polarization for the zeroth order diffraction of a Gaussian beam because of the geometry of the groove. The grooves of the elliptical grating are much more "straight" than the ones of the plane grating. Thus the incident wave polarization remains mainly a TM mode over the entire surface of the grating and the diffracted beam suffers much less distortion and cross-polarization due to the generation of the TE mode. The same argument can be used to explain the difference in cross-polarization between the two plane gratings #1 and #2. As indictated in Table I, the difference between R_{TE} and R_{TM} is much less in the case of grating #2 than in grating #1. The two polarizations are therefore reflected with about the same reflection coefficient, and less cross-polarization is generated.

It is important to point out that both numerically and experimentally we consider only the quantities of C^2 and XP, which do not include the phase distribution of the diffracted wave. A good beam quality at a given location does not require that this property to be conserved along its propagation path and the pattern can be deformed by astigmatism. In principle, the spatial phase distribution should also be plotted. However, from an experimental point of view, such a measurement, while in principle feasible, is a complex one. Instead, we have followed the beam pattern along the axis z' both in the numerical calculations and in the experiment. The numerical results are presented on Fig. 19 for an elliptical grating. We note that the beam quality does not vary as it propagates. The Gaussian content

C^2 remains constant, showing that the astigmatism of the diffracted beam is negligible. A similar observation was found during the cold test.

IV. CONCLUSIONS

We have presented measurements and an analysis of the distortion and cross-polarization of a Gaussian beam which is diffracted in zeroth order by a grating mounted in a -1 Littrow arrangement. The grating geometry is designed for output coupling from (or input coupling to) a Fabry-Pérot resonator. It was found experimentally that an elliptical grating provides the best results, in agreement with numerical simulations.

ACKNOWLEDGMENTS

This work is supported in part by the Office Fédéral de l'Energie under grants OFEN-EF-FUS(91)-01, and OFEN-Gyrotron 581 233, and by the Fonds National Suisse pour la Recherche Scientifique.

We would like to acknowledge fruitful discussions with Professors N. Gallagher (Purdue University) and R. Petit (University of Marseille). Ms. M. Roulin performed the measurement presented in Fig. 16 and has verified experimentally the Gaussian shape of the TEM_{oo} mode in a resonator using a grating as an output coupler. A critical reading of the manuscript was performed by Drs. M. Henderson and D. Whaley.

REFERENCES

1 R.L. Abrams, IEEE J. Quant. Electronics **QE-8**, 838 (1972).
L. Rebuffi and J.P. Crenn, Int. J. Infrared and Millimeter Waves **10**, 291 (1989).

2 S.N. Vlasov et al., Radio Eng. Electron. Phys. **20**, 14 (1975).
A.V. Gaponov and M.I. Petelin, Int. Workshop on Strong Microwaves in Plasmas, Suzdal, USSR, 1990, to be published.
B.W. Stallard et al., Int. J. Infrared and Millimeter waves **11**, 1011 (1990).

3 See, for example, S. Alberti et al., Phys. Fluids **B2**, 1654 (1990); A.W. Fliflet et al., J. Fusion Energy **9**, 31 (1990) and references therein.
M. Blank et al., Int. J. Electronics **72**, 1093 (1992).

4 M.E. Read et al., Int. J. Electronics **65**, 309 (1989).

5 J.Ph. Hogge et al., 15th Int. Conf. Infrared and Millimeter Waves, Orlando, Florida, R. Temkin ed., **SPIE 1514**, 535 (1990).

6 J.Ph. Hogge et al., 16th Int. Conf. Infrared and Millimeter Waves, Lausanne, Switzerland, M.R. Siegrist, M.Q. Tran and T.M. Tran, editors, **SPIE 1576**, 540 (1991).

7 R. Petit, Electromagnetic Theory of Gratings, Ed. Springer Verlag (1980).

8 T.M. Tran et al., IEEE Trans. Electron. Dev. **36**, 1983 (1989).

9 A. E. Siegman, Lasers, University Science Books (1986).

10 M.E. Read, Millimeter Wave Technology and Radio Frequency Power Science, **SPIE 791**, 46 (1987).

11 K.E. Kreischer et al., IEEE Trans. Plasma Sci. **13**, 364 (1985).

12 S. Alberti et al., Phys. Fluids **B2**, 2544 (1990).

13 See, for example, Jin Au Wong, Electromagnetic Theory, Ed. J.Wiley and Sons Inc. (1990) p. 443.

14 J.A. Stratton and L.J. Chu, Phys. Rev. **56**, 99 (1939).

15 A. Perrenoud et al., Int. J. Electron. **57**, 985 (1984).

16 A. Wirgin and R. Deleuil, J. Opt. Soc.Am. **59**, 1348 (1969).

17 B. Jödicke et al.,15th Int. Conf. Infrared and Millimeter Waves, Orlando, Florida, R. Temkin ed., **SPIE 1514**, 321 (1990).

18 J.A. Murphy, Int. J. Infrared and Millimeter Waves **8**, 1165 (1987).

Parameters	Plane grating with straight grooves	Plane grating with curvilinear grooves #1	Plane grating with curvilinear grooves #2	Ell. grating with curvilinear grooves
Angle of incidence θ	36.87°	45°	28°	28°
Groove depth h/d	0.30	0.36	0.38	0.38
Mirror separation D	80.5 mm	338 mm	216 mm	400 mm
Diameter of spherical mirror	140 mm	84 mm	70 mm	100 mm
Curvature radius of spherical mirror R_c	1160 mm	200 mm	140 mm	235 mm
Beam waist kw_0	35.2	19.3	15	18
Spot-size on the grating kw_m	35.2	47.9	31.6	35.6
Polarization	TM	TM	TM	TM
Zeroth order efficiency R_{TM}	10%	2%	10%	10%
Zeroth order efficiency R_{TE}	7%	80%	27%	27%
Fresnel number N	20.3	2.	1.75	1.92
Resonator parameter g	0.93	-.7	-.55	-.7
Focal length f of the grating	-	-	-	186 mm
w_m/f	-	-	-	0.130
Design frequency	100 GHz	120 GHz	92.4GHz	92.4 GHz
Output beam waist kw_1	42.72	51.27	39.48	39.48

Table 1: Parameters of the different resonators

	Plane grating #2		Elliptical grating	
	Theory	Exp.	Theory	Exp.
Gaussian content C^2	90%	90%	98%	99%
Cross-Polarisation content XP	6%	(6.9%)	0.6%	3%

TABLE II - Comparison between the computed properties of the grating and the measured ones. The cross-polarization content in the case of the plane grating was measured in a set-up which uses an additional focusing elliptical mirror. The parameters of the grating are given in the third and fourth column of Table I

FIGURE CAPTIONS

FIG. 1. Geometry of the grating, resonator and the electromagnetic beam. The experimental set-up and the differenrt coordinate systems are also shown.

FIG 2 Contours of efficiency for the -1 order at the fundamental versus the angle of incidence θ and the normalized groove depth h/d, for a sinusoidal grating in a Littrow mount: case (a) TE and case (b) TM. Theta is the angle of incidence θ, h and d are the groove depth and the grating period respectively.

FIG. 3. Geometry of grating. The lines ϕ = constant are the phase fronts of the incident wave.

Fig. 4 Contours of efficiency for the -2 order at the second harmonic versus the angle of incidence θ and the normalized groove depth h/d, for a sinusoidal grating in a Littrow mount: case (a) TE, case (b) TM.

FIG 5. A plane grating with curved grooves. The lines on Fig. 5(a) represent the highest point of the grooves. The grating is viewed from above. A picture of an actual grating is shown in Fig. 5(b). The groove shape is sinusoidal.

FIG. 6. An elliptical grating. The lines on Fig. 6(a) represent the highest point of the grooves. The grating is viewed from above. A picture of an actual grating is shown in Fig. 6(b). The groove shape is sinusoidal.

FIG. 7. Local coordinate system on the grating. The incident $\underline{E}^i$ and $\underline{B}^i$ fields are neither pure TE nor TM modes.

FIG. 8 Two-way loss T as a function of frequency for a plane grating with straight grooves. Squares: $kw_m = 35.6$, Triangles: $kw_m = 18.9$.

FIG. 9 Angular pattern of the output from a resonator with a plane grating. The angle value of 0 corresponds to the zeroth order diffraction angle.

FIG. 10 RF power contour plot of a Gaussian beam diffracted by a plane grating with straight grooves. The cross gives the location of the maximum and the contour lines are separated by 1 dB.

FIG. 11 Pattern of a TEM_{00} mode measured at the entrance of the corrugated waveguide. The polarization is the correct one. The grating is plane with curvilinear grooves. Contours are separated by 3 dB. (a) Power contour plot (b) Theoretical contour plot of the optimal Gaussian beam.

FIG. 12 Power contour plot of the cross-polarized signal of Fig. 11(a). The grating is plane with curvilinear grooves. The lines are separated by 1 dB.

FIG. 13 Power contour plot after 2 m of propagation in an HE_{11} waveguide. The detector is placed at 1 m from the aperture. The lines are separated by 2 dB. (a) measured contours, (b) theoretical contours.

FIG. 14 Correct polarization power contour plot of a TEM_{00} mode measured at the focal point. The grating is elliptical. The lines of equal intensity are separated by 2 dB. (a) and (b) correspond to the measured and calculated pattern respectively.

FIG. 15 Cross-polarization power contour plot of a TEM_{00} mode measured at the focal point. The grating is elliptical. (a) and (b) correspond to the measured and calculated pattern respectively. The lines of equal intensity are separated by 1 dB.

FIG. 16 Two-way loss T of the TEM_{00} modes as a function of frequency for the ellipsoidal grating. Angle of incidence: circles: $\theta = 28°$, triangles: $\theta = 27°$.

FIG. 17 Correct polarization power contour plot of the RF diffracted from a plane grating. The lines of equal intensity are separated by 2 dB. (a) and (b) correspond to the measured and calculated pattern respectively.

FIG. 18 Cross-polarization power contour plot from a plane grating. The lines of equal intensity are separated by 1 dB. (a) and (b) correspond to the measured and calculated pattern respectively. The measured signal is too weak to allow a precise determination of the content in the cross-polarization XP.

FIG. 19 Calculated variation of the spot size w' and the gaussian content along the path of the output beam. The solid line corresponds to the variation of the spot size w' and the dashed line to the gaussian content

C^2. The calculated spot size corresponds exactly to the one predicted by Eq. (5).

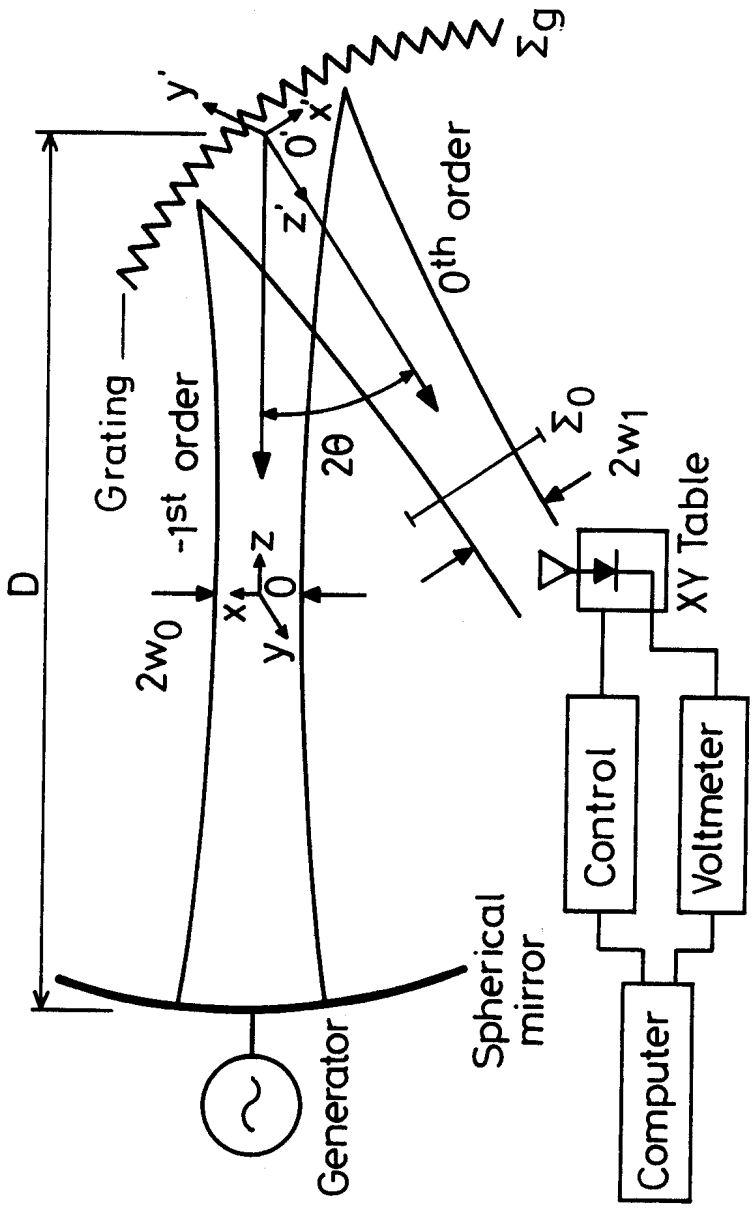
Σg
y'
x'
0'
z'
0th order
Grating
-1st order
D
2w0
x
z
0
y
2θ
Σ0
2w1
XY Table
Control
Voltmeter
Computer
Spherical mirror
Generator

Fig. 1

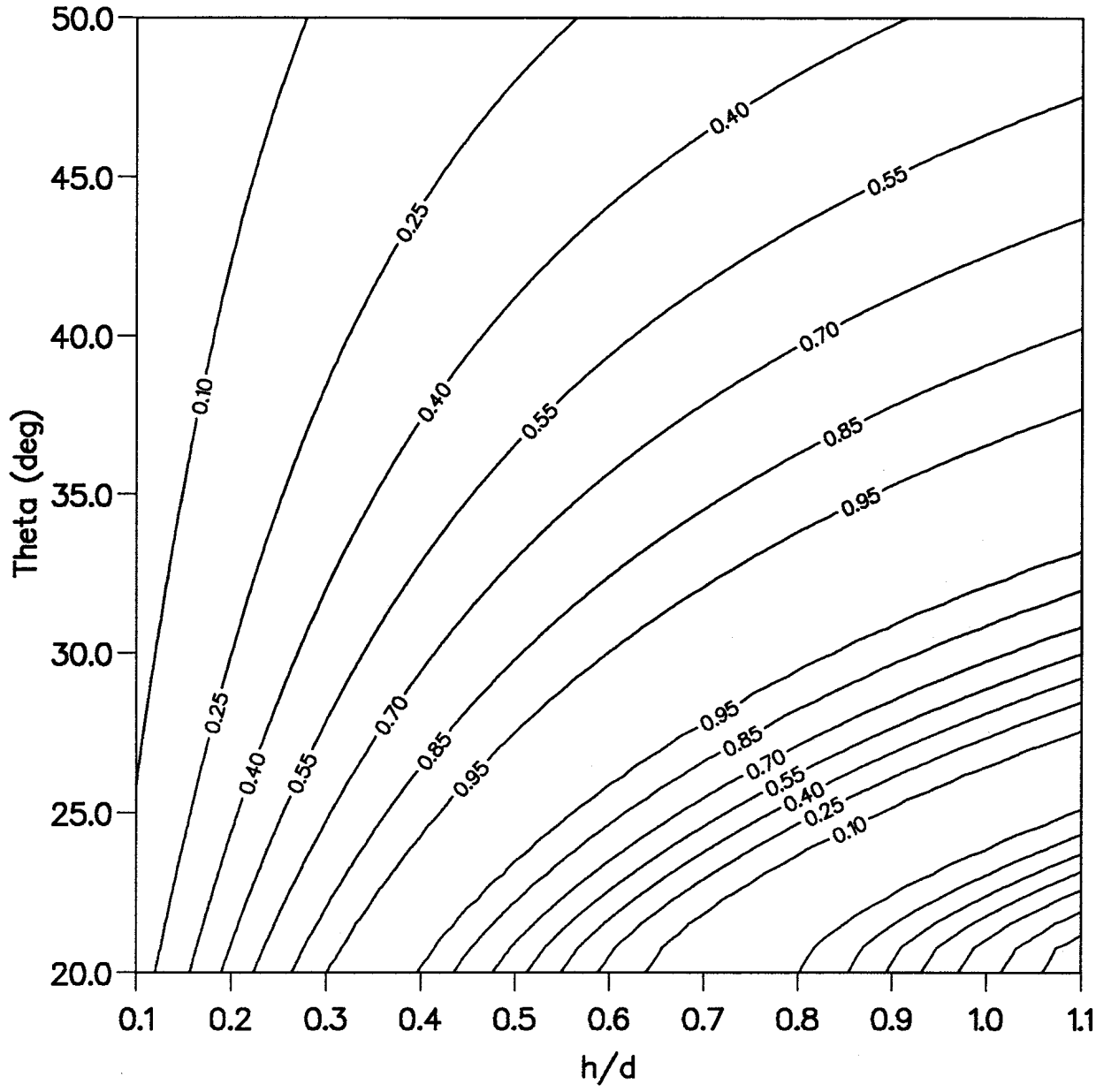
50.0
45.0
40.0
35.0
30.0
25.0
20.0
Theta (deg)
0.1
0.2
0.3
0.4
0.5
0.6
0.7
0.8
0.9
1.0
1.1
h/d
0.10
0.25
0.40
0.55
0.70
0.85
0.95

FIG. 2(a)

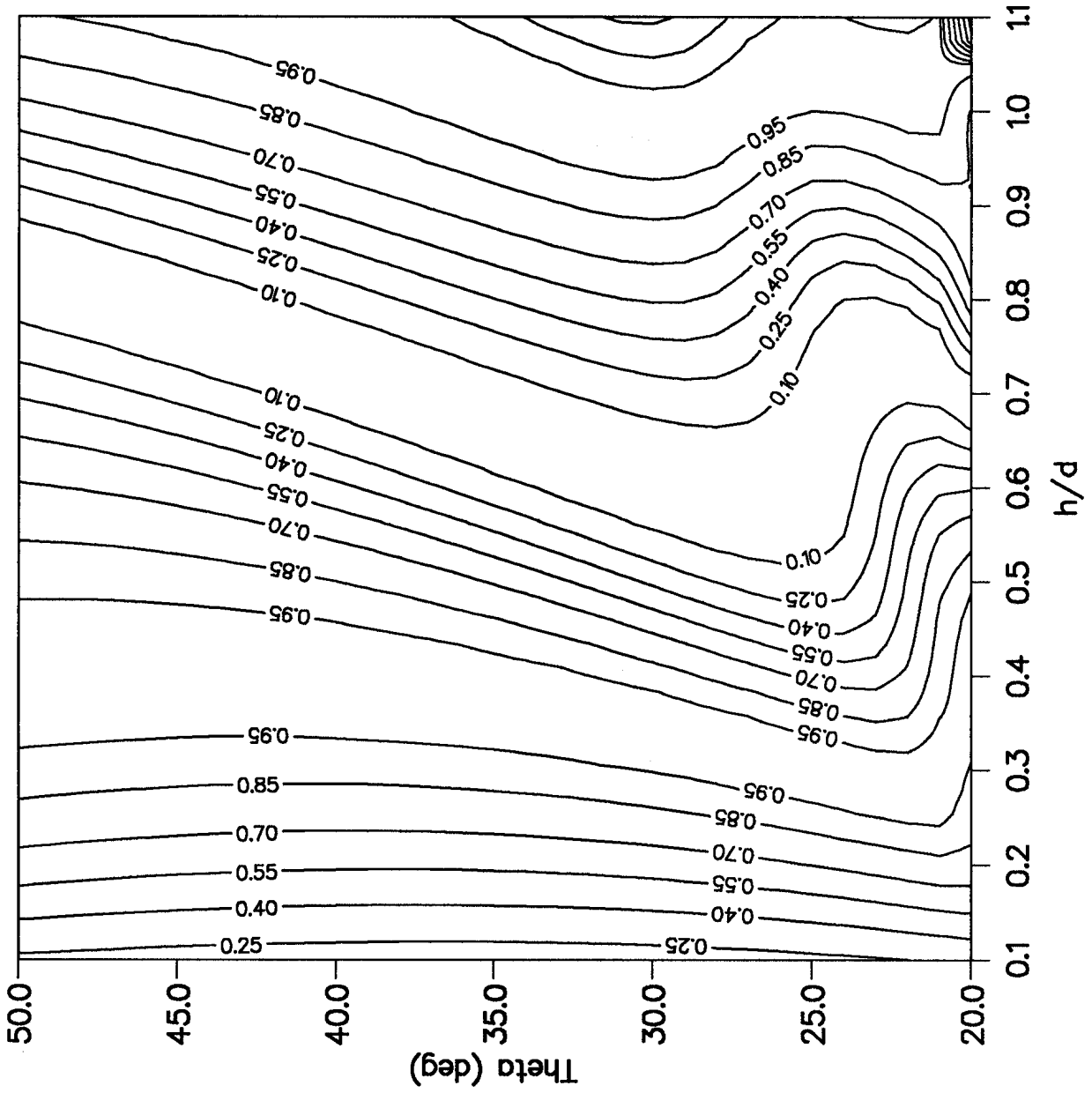
Theta (deg)
50.0
45.0
40.0
35.0
30.0
25.0
20.0
h/d
0.1
0.2
0.3
0.4
0.5
0.6
0.7
0.8
0.9
1.0
1.1
0.95
0.85
0.70
0.55
0.40
0.25
0.10

FIG. 2(b)

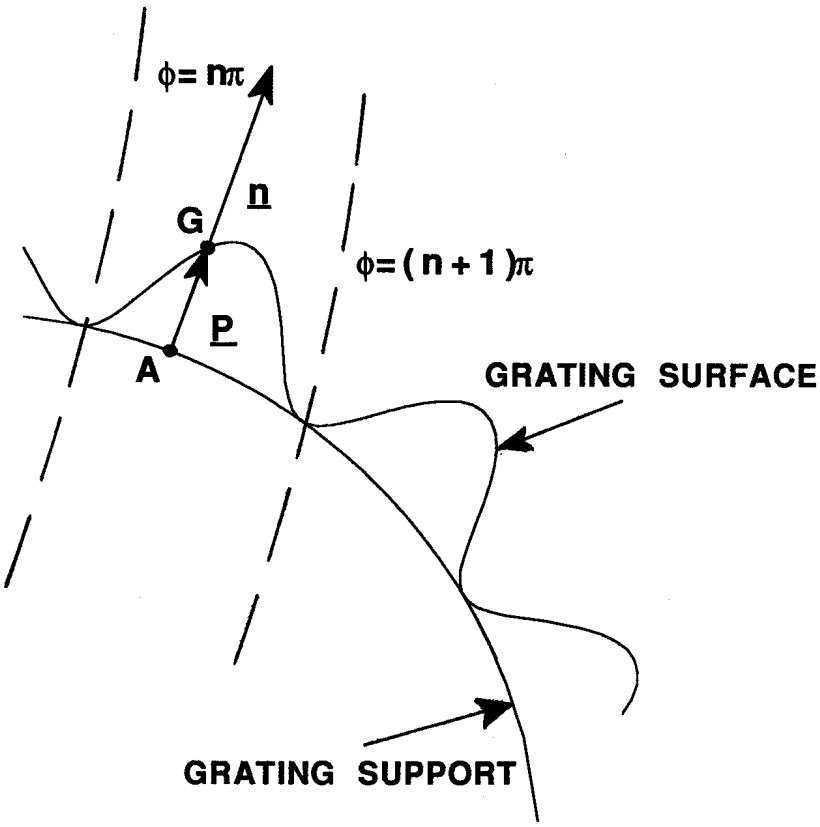

FIG. 3

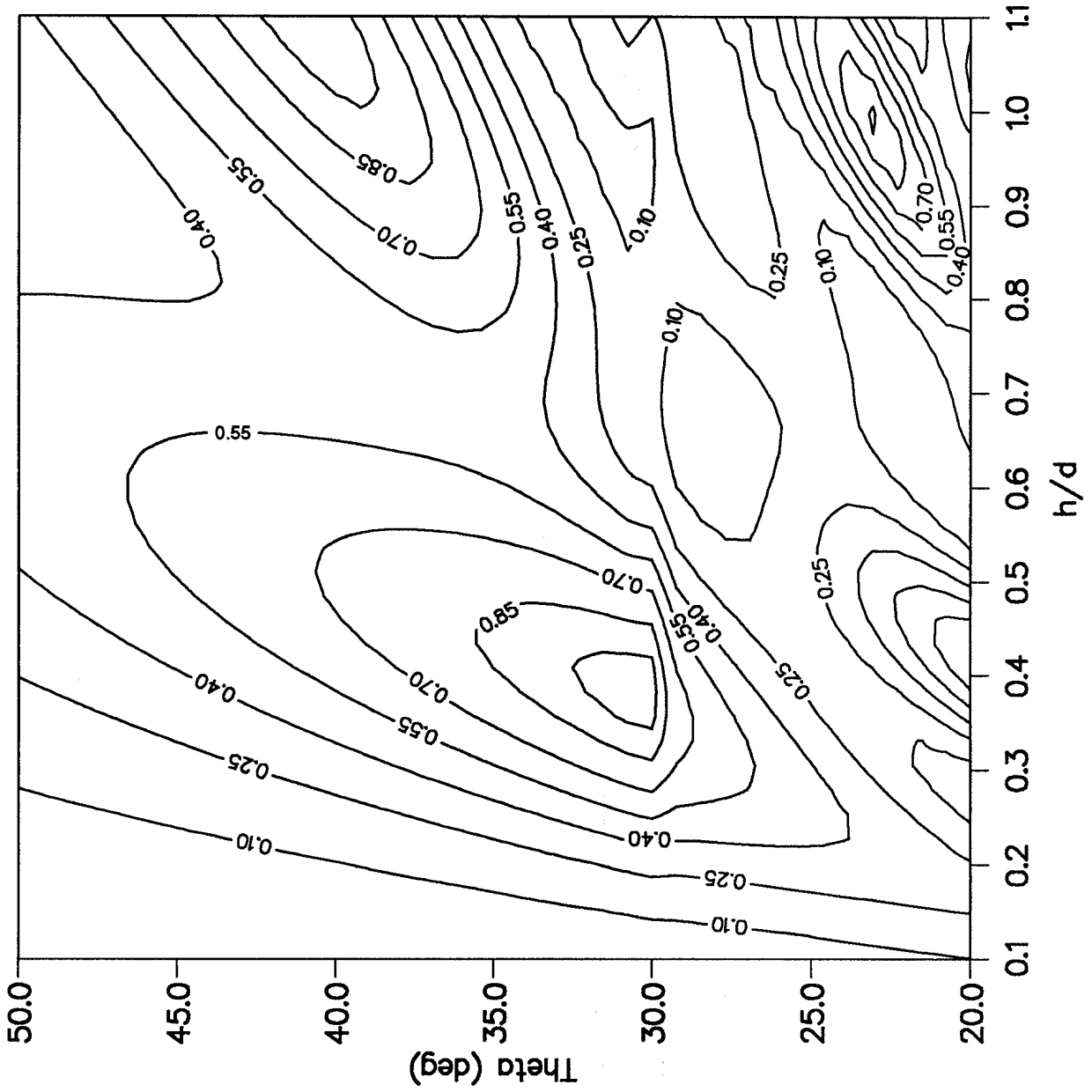
Theta (deg)
50.0
45.0
40.0
35.0
30.0
25.0
20.0
h/d
0.1
0.2
0.3
0.4
0.5
0.6
0.7
0.8
0.9
1.0
1.1
0.10
0.25
0.40
0.55
0.70
0.85

FIG. 4(a)

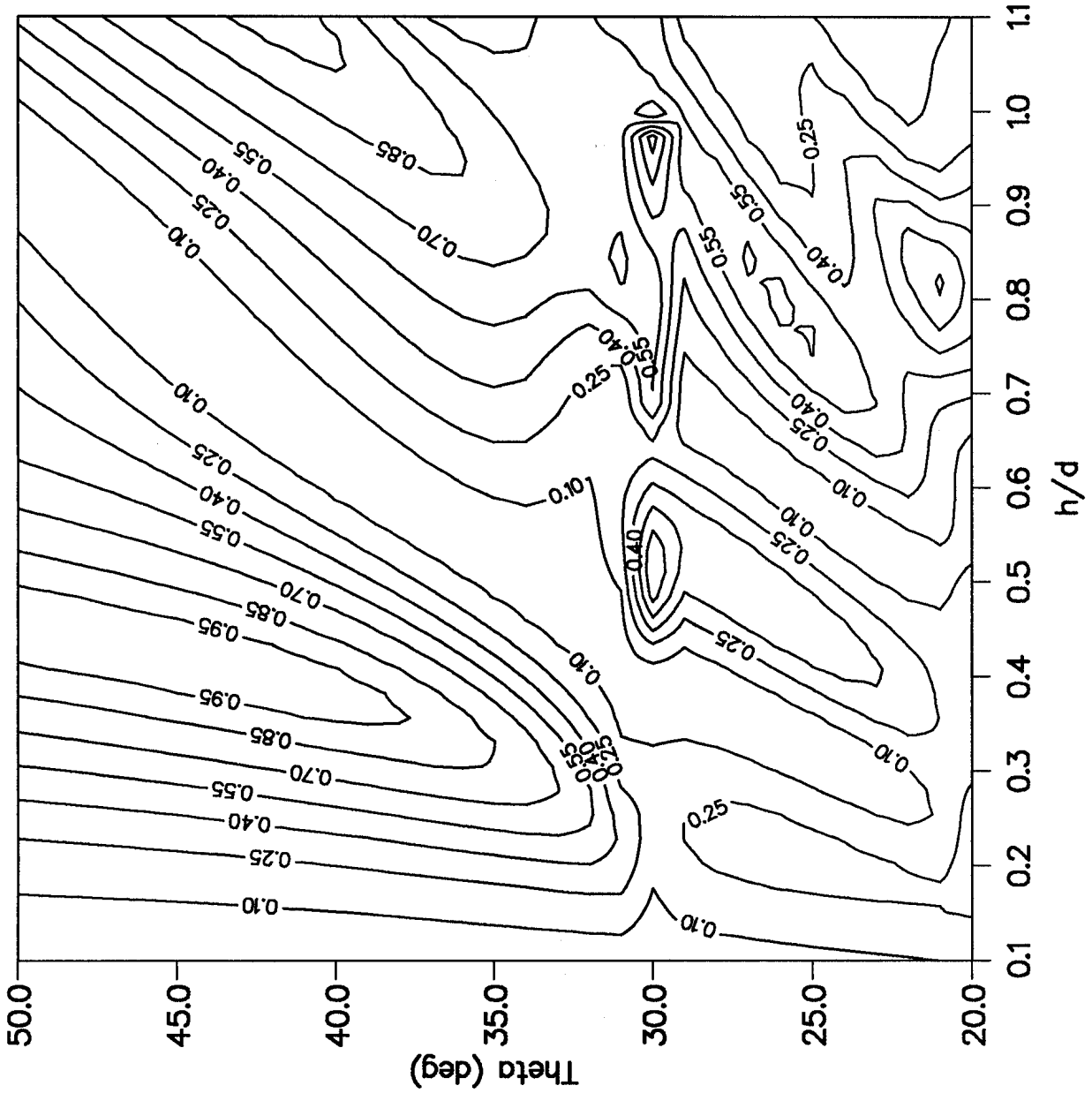
Theta (deg)
50.0
45.0
40.0
35.0
30.0
25.0
20.0
h/d
0.1
0.2
0.3
0.4
0.5
0.6
0.7
0.8
0.9
1.0
1.1
0.10
0.25
0.40
0.55
0.70
0.85
0.95

FIG. 4(b)

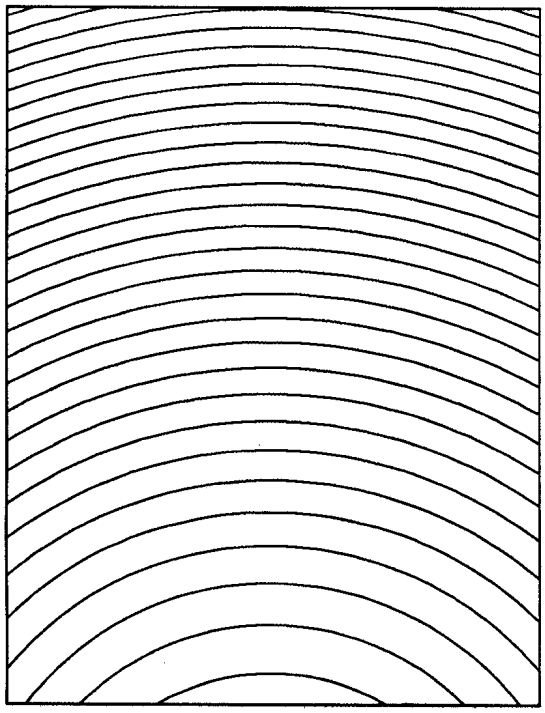

FIG. 5(a)

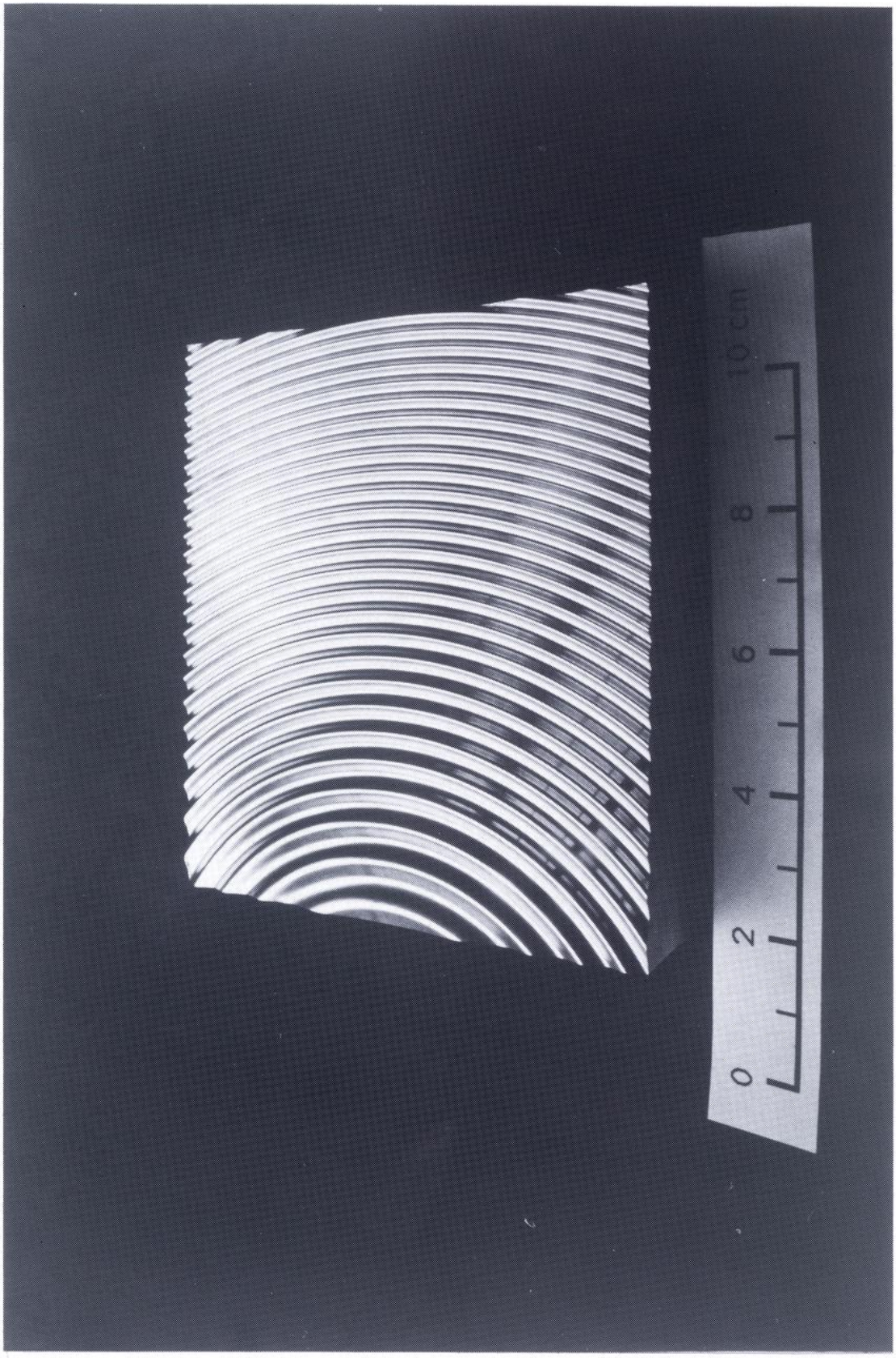

FIG. 5(b)

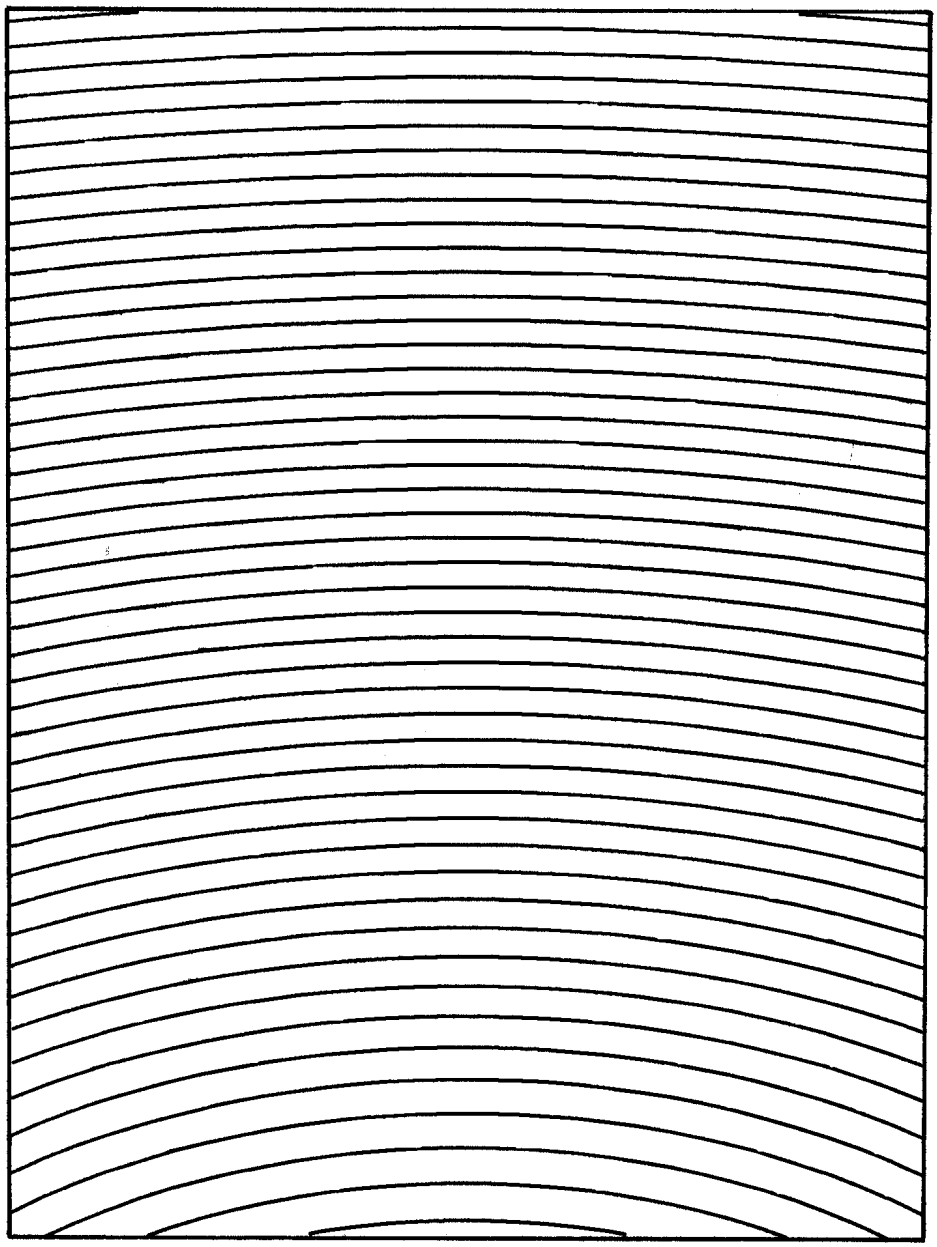

FIG. 6(a)

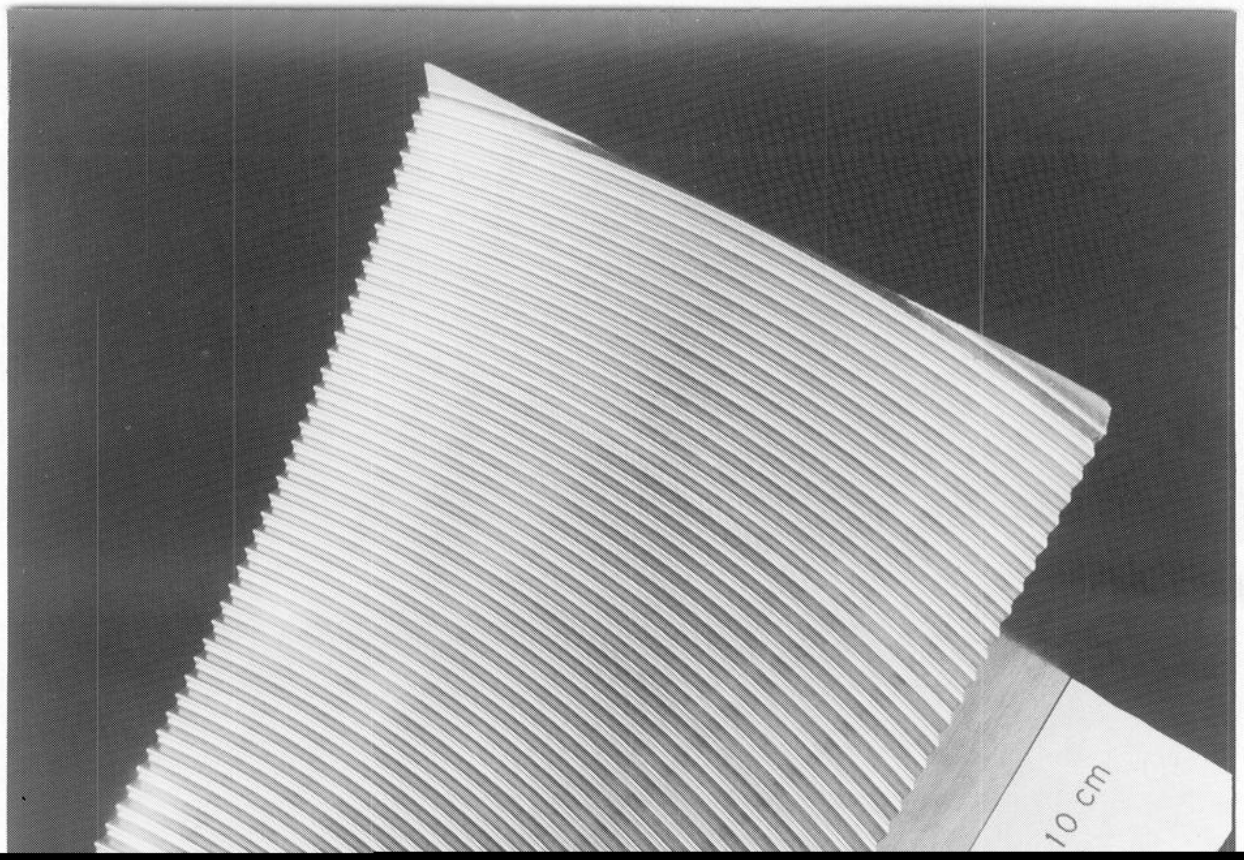
10 cm

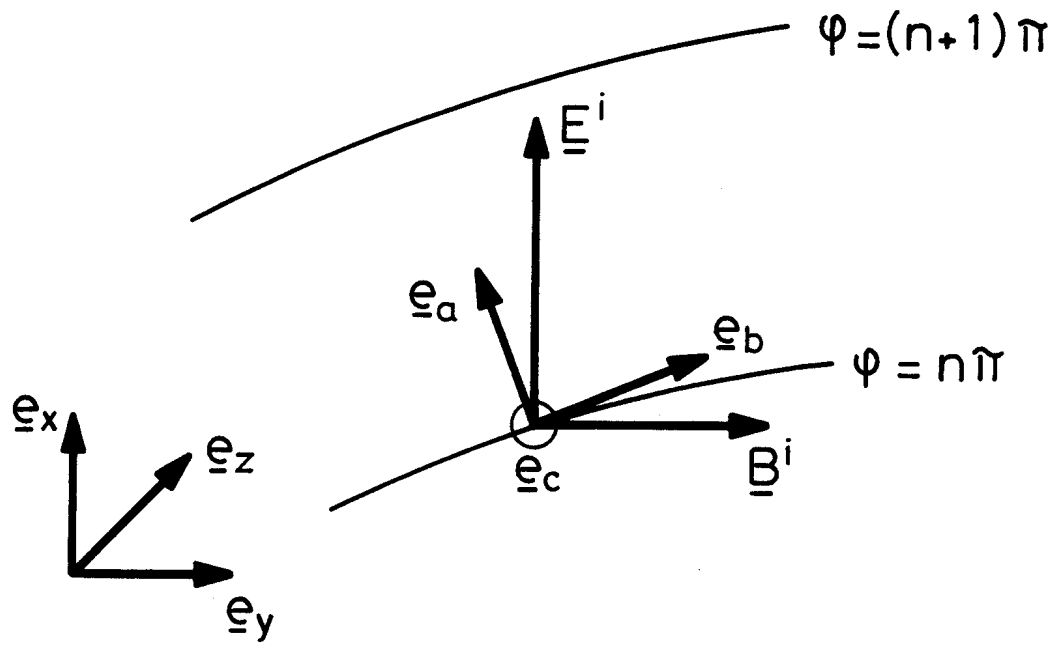

FIG. 7

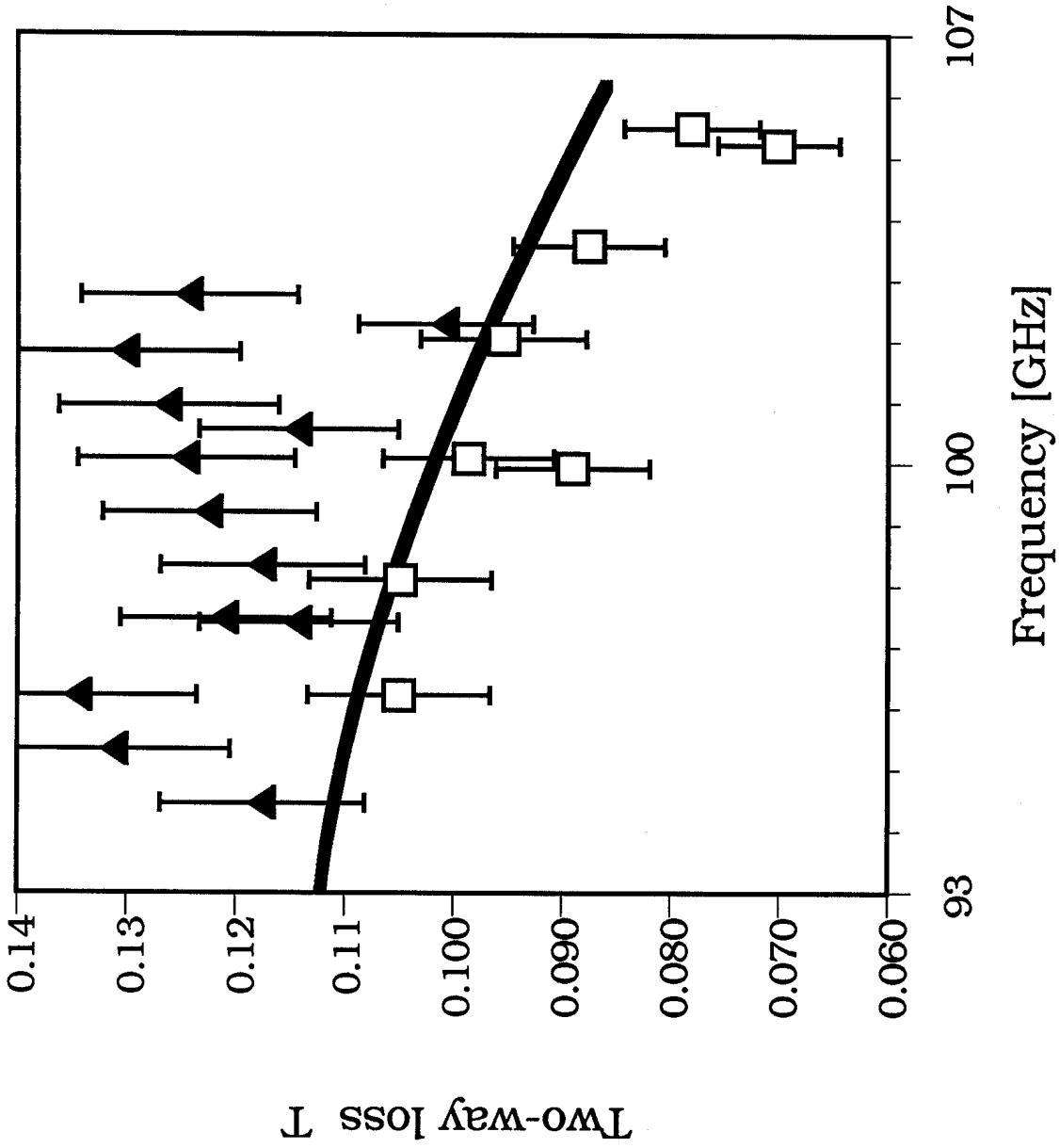
Two-way loss T
0.14
0.13
0.12
0.11
0.100
0.090
0.080
0.070
0.060
93
100
107
Frequency [GHz]

FIG. 8

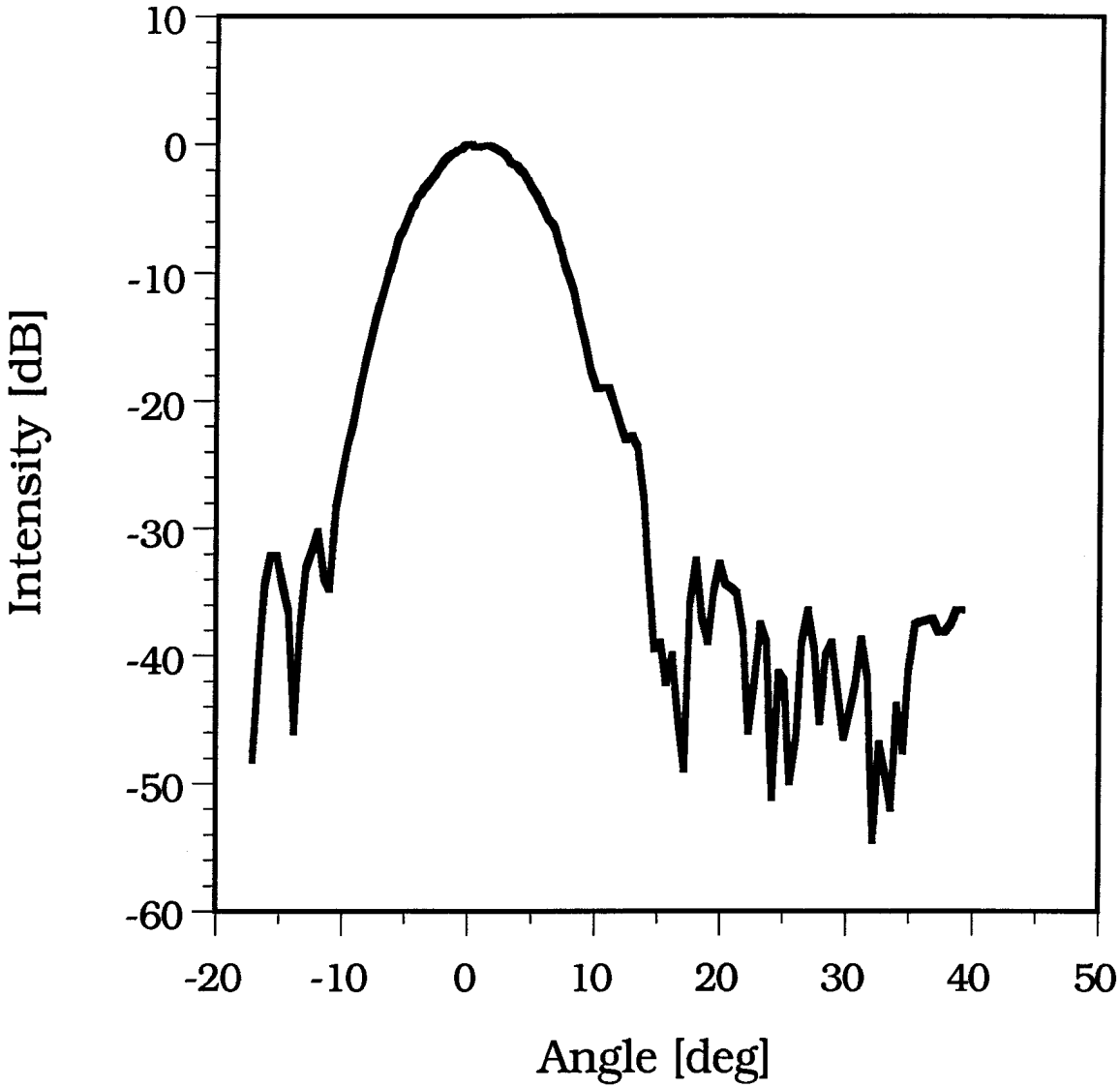

FIG. 9

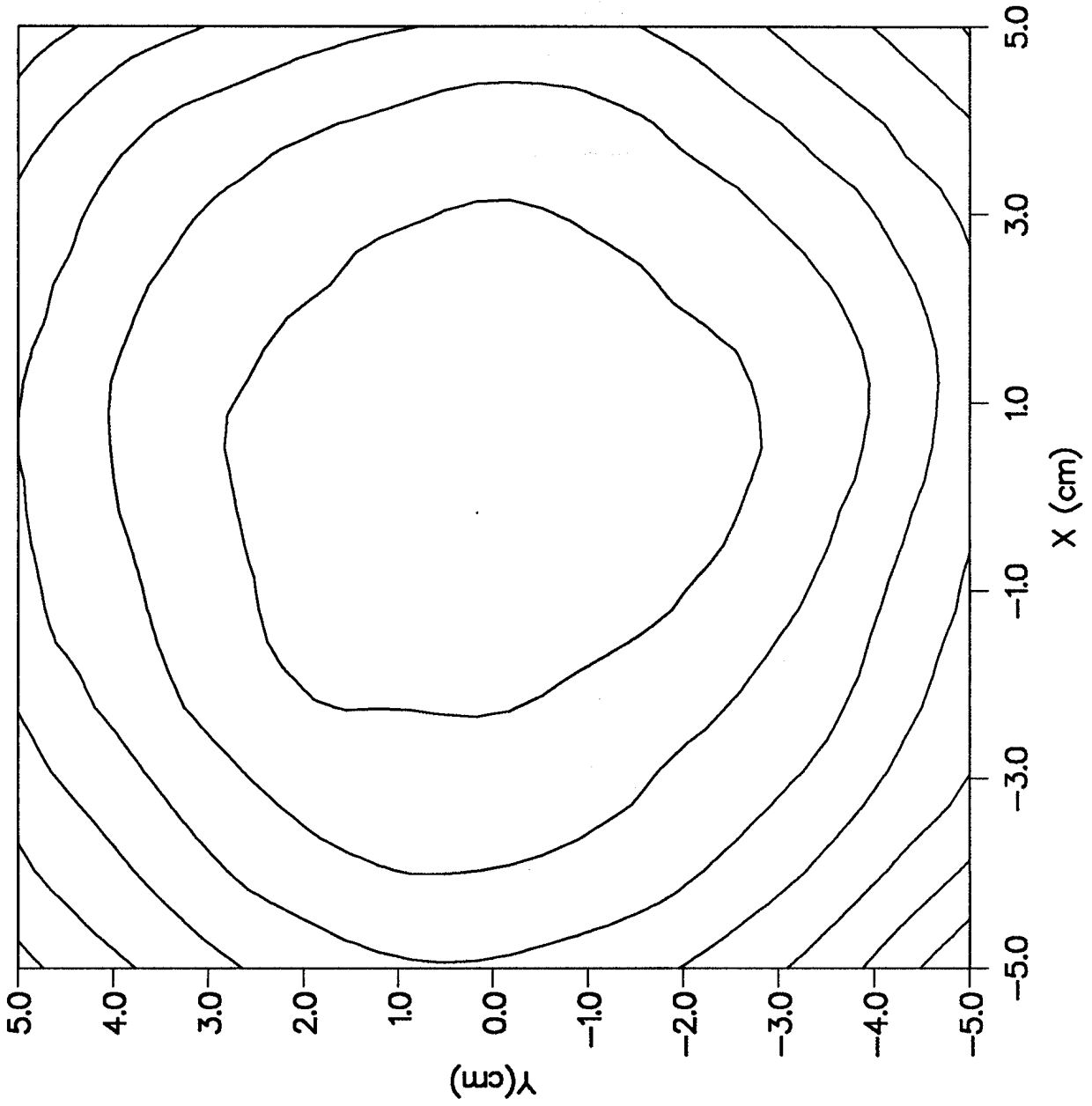

FIG. 10

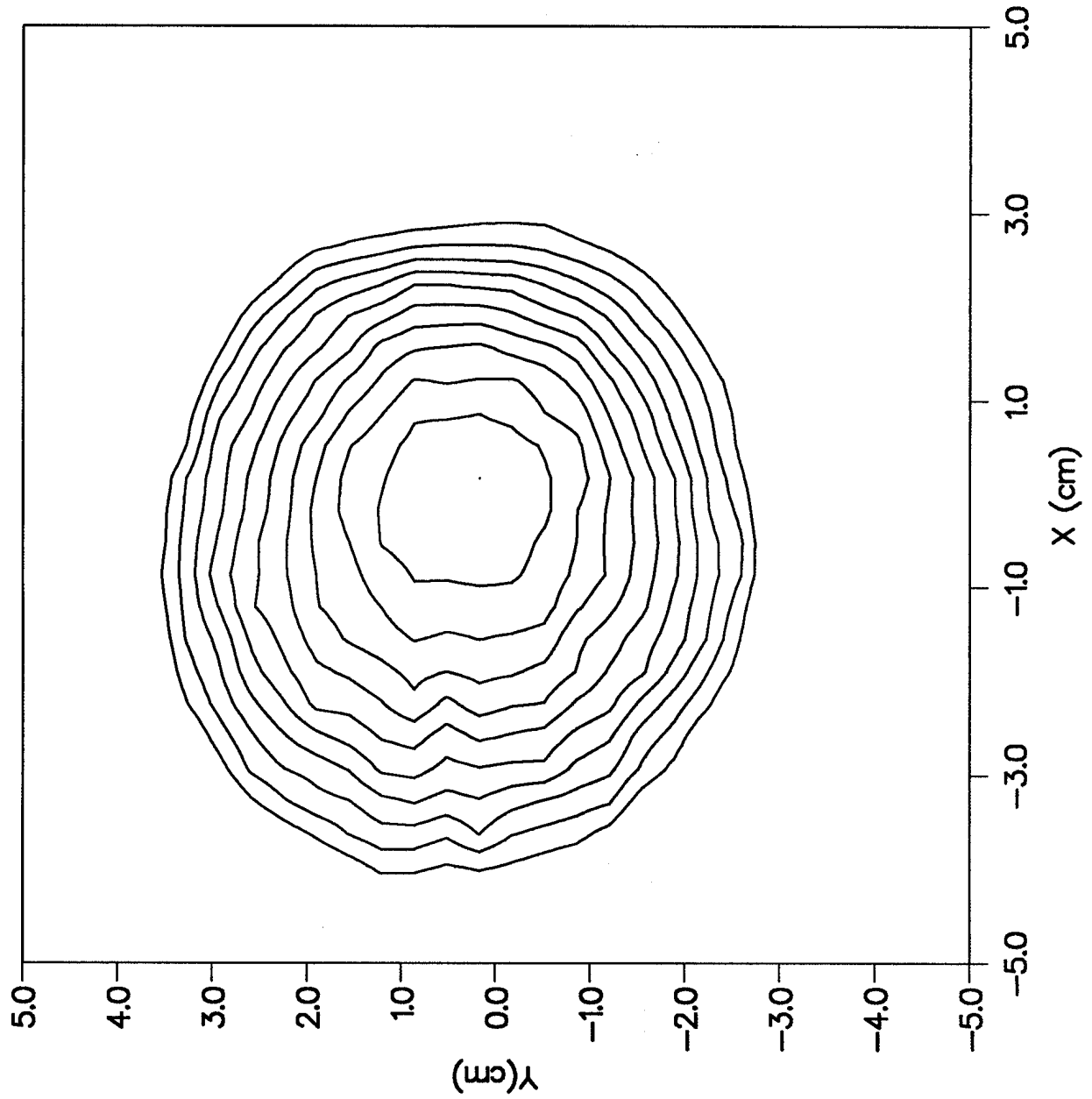

FIG. 11(a)

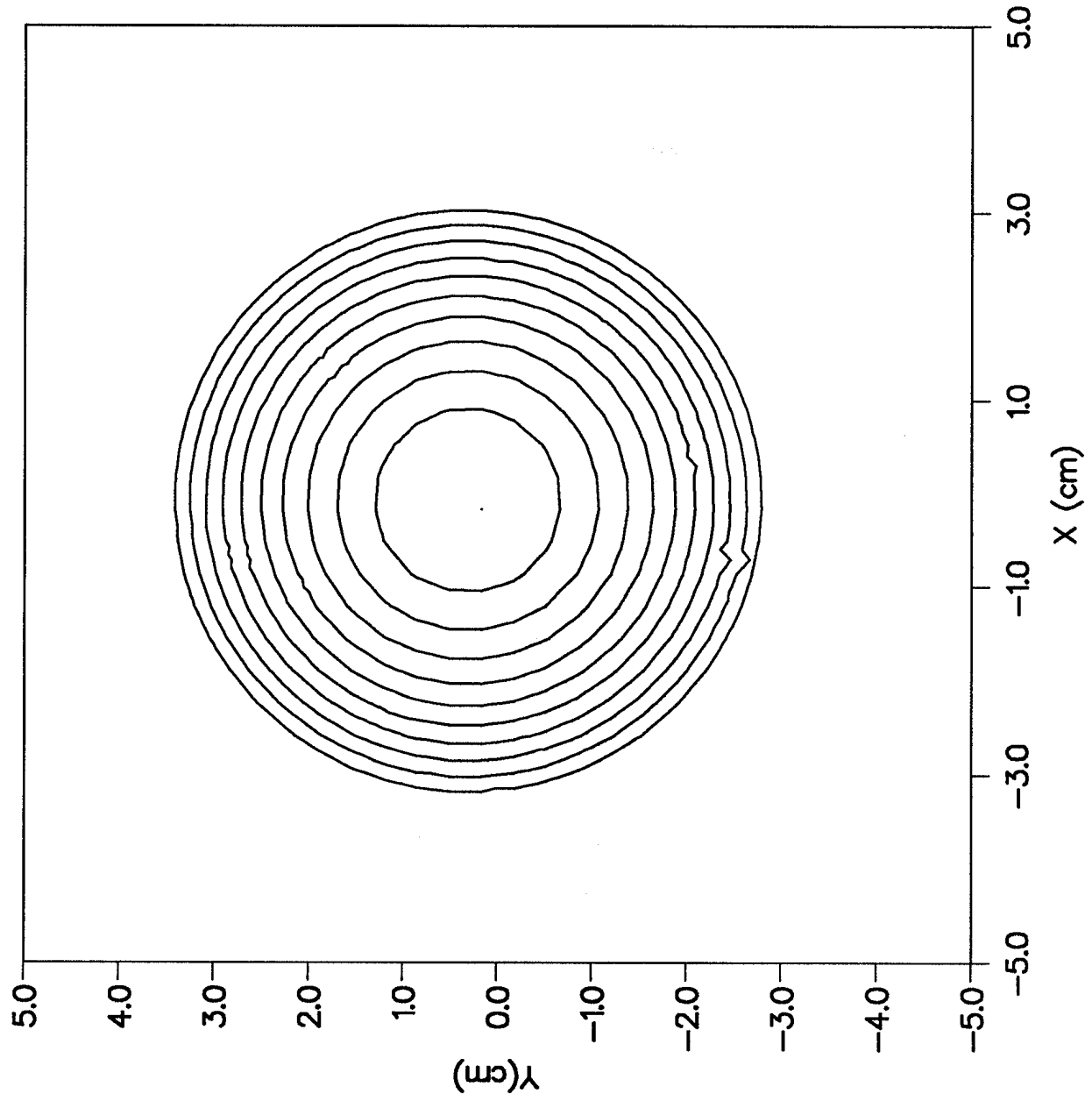

FIG. 11(b)

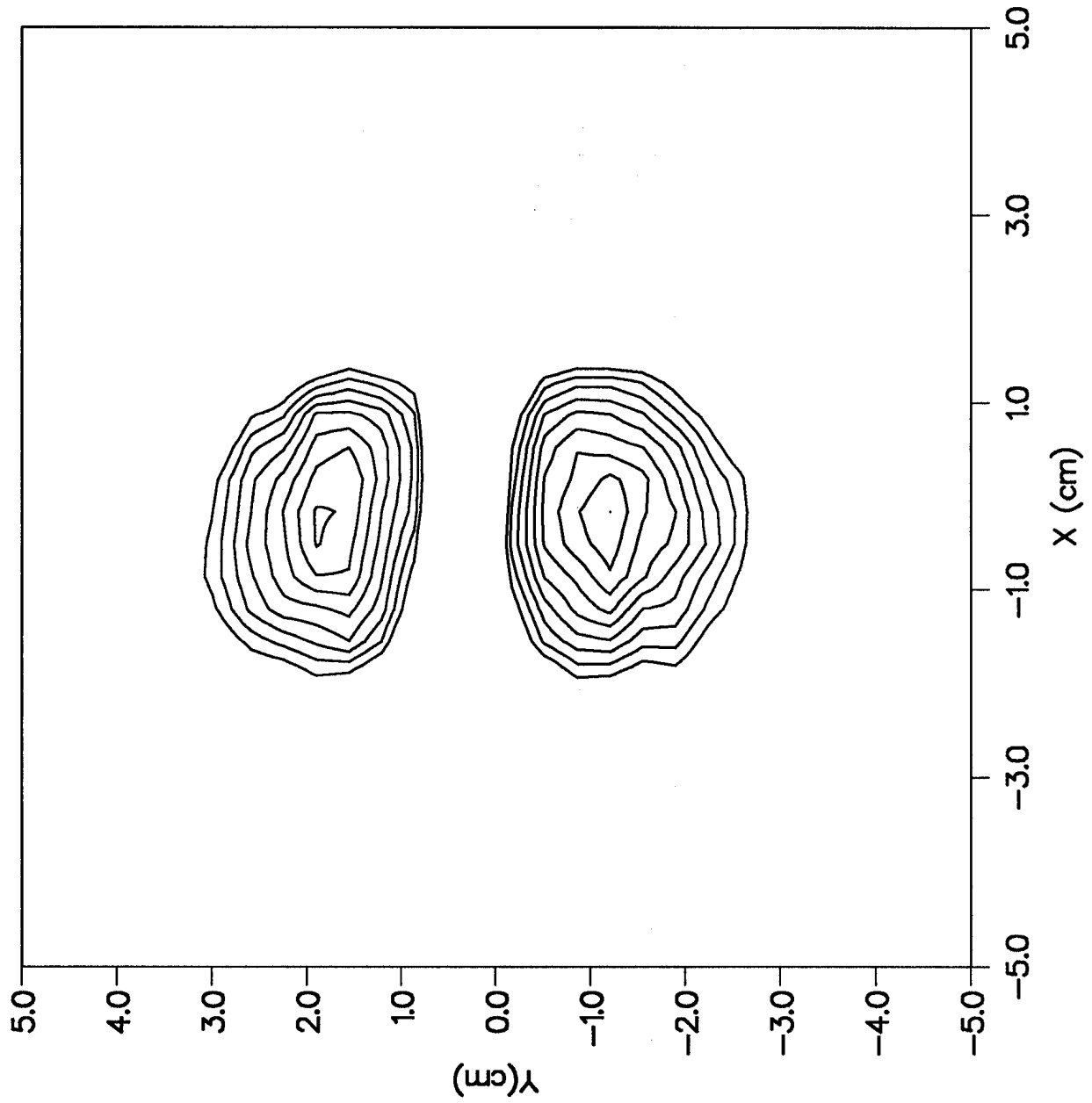

FIG. 12

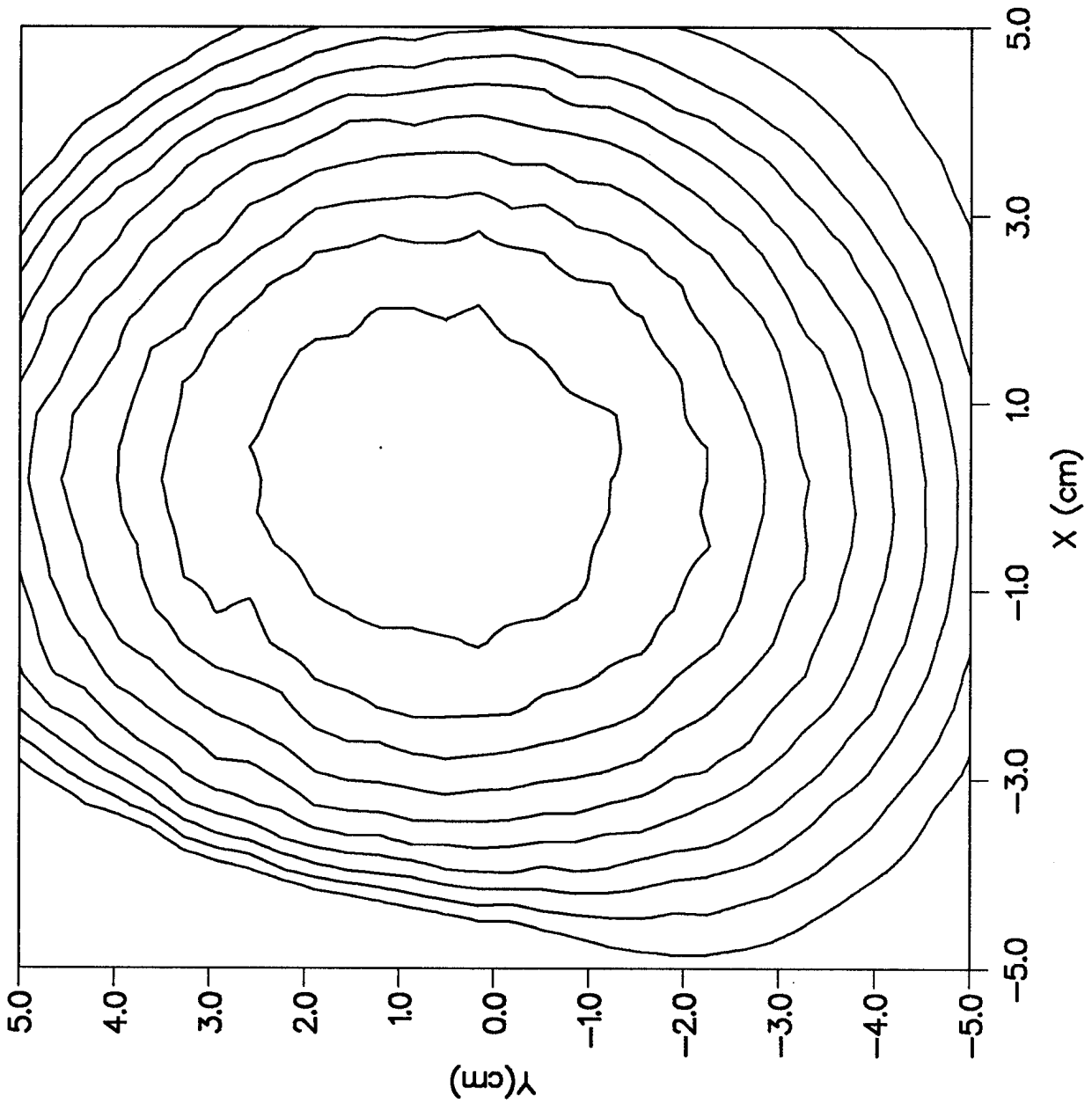

FIG. 13(a)

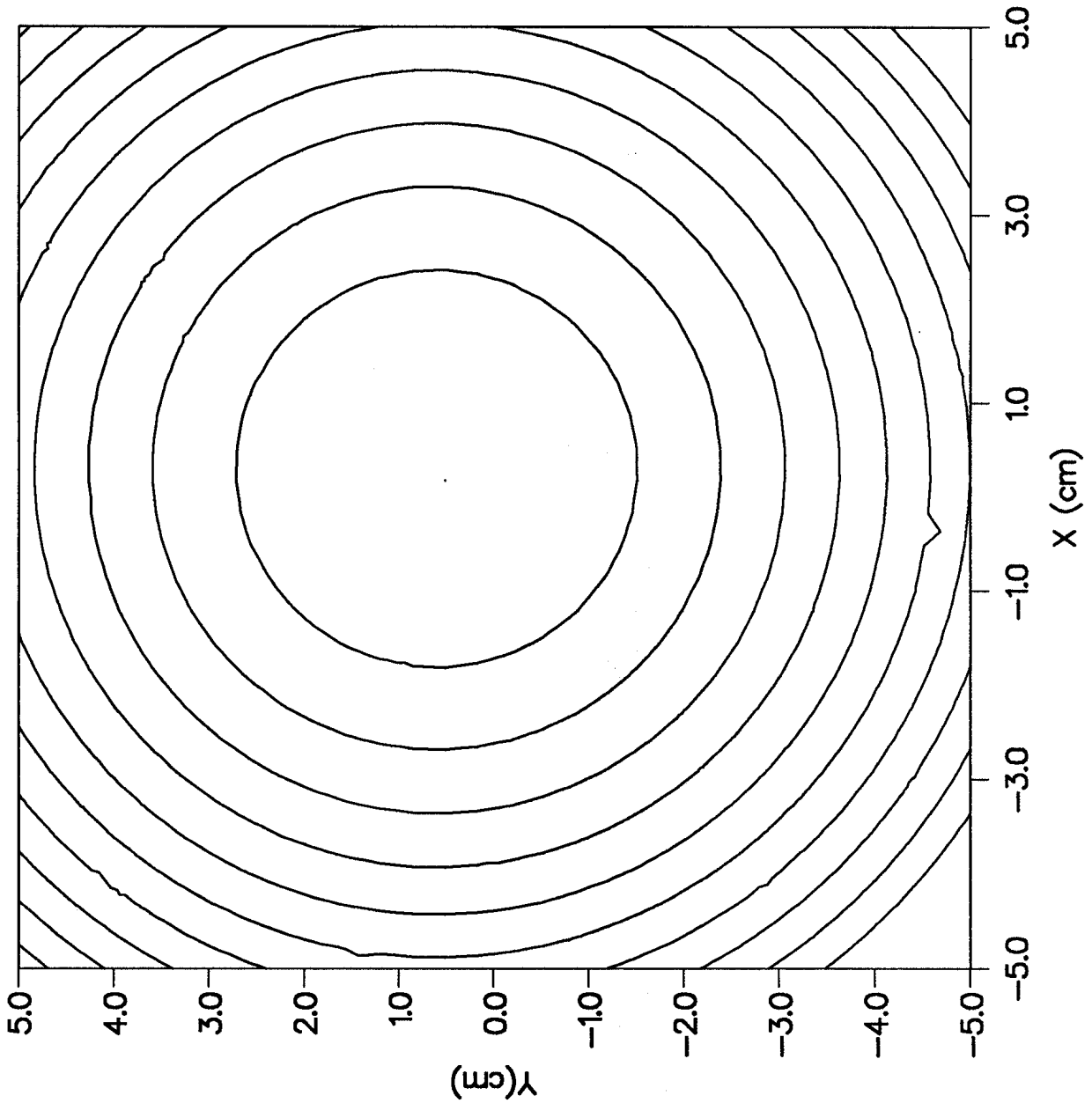

FIG. 13(b)

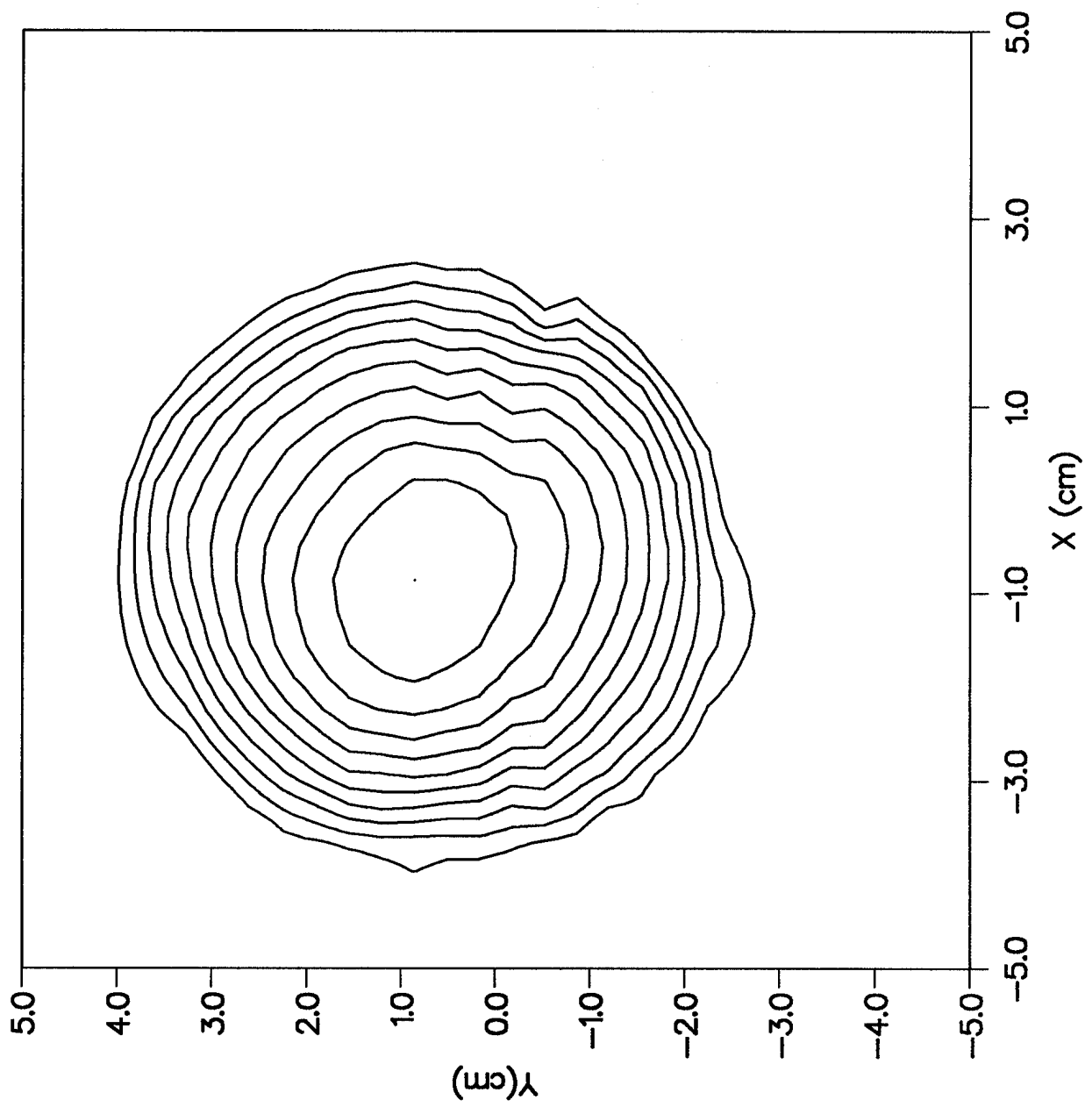

FIG. 14(a)

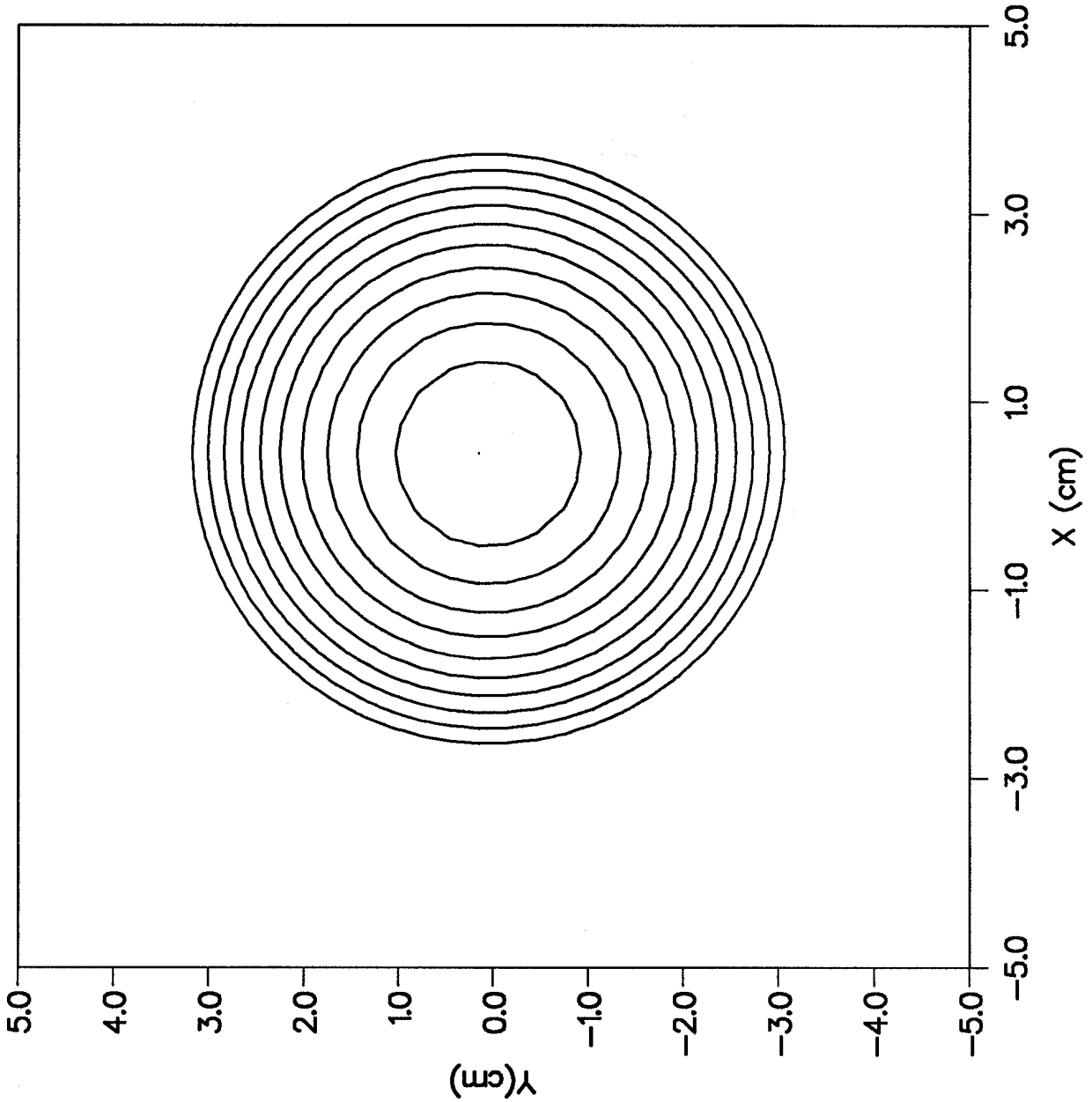

FIG. 14(b)

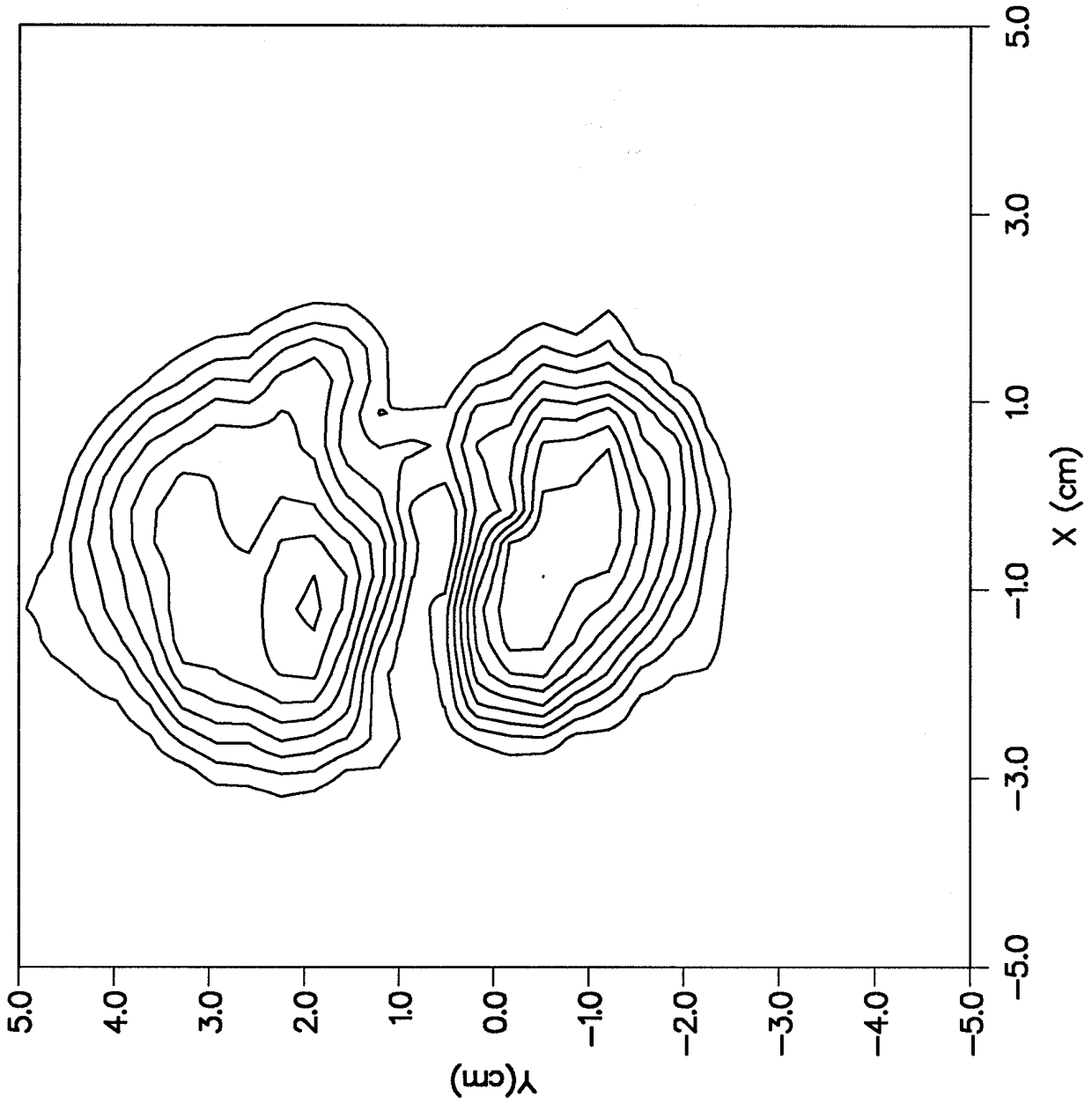

FIG. 15(a)

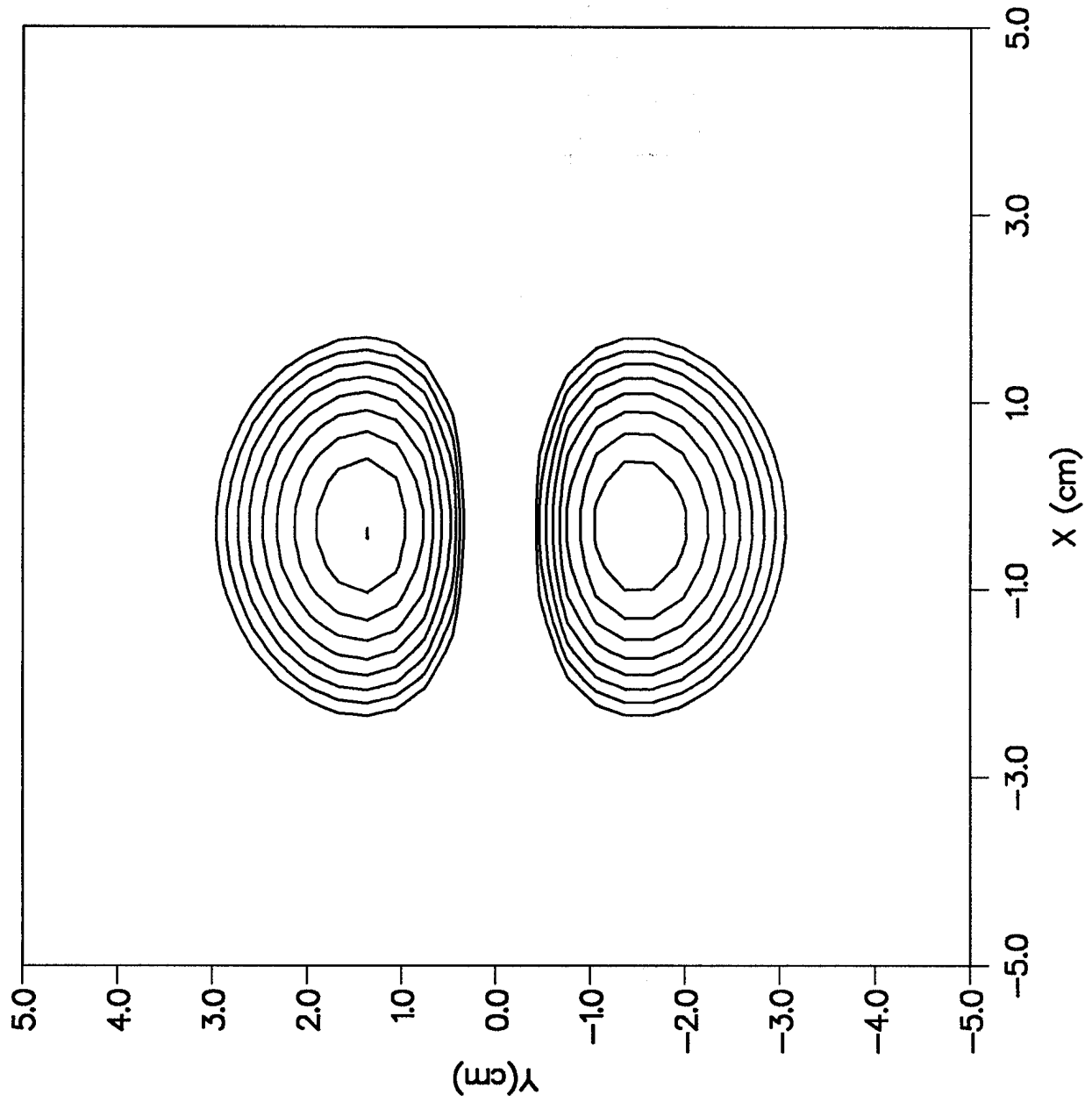

FIG. 15(b)

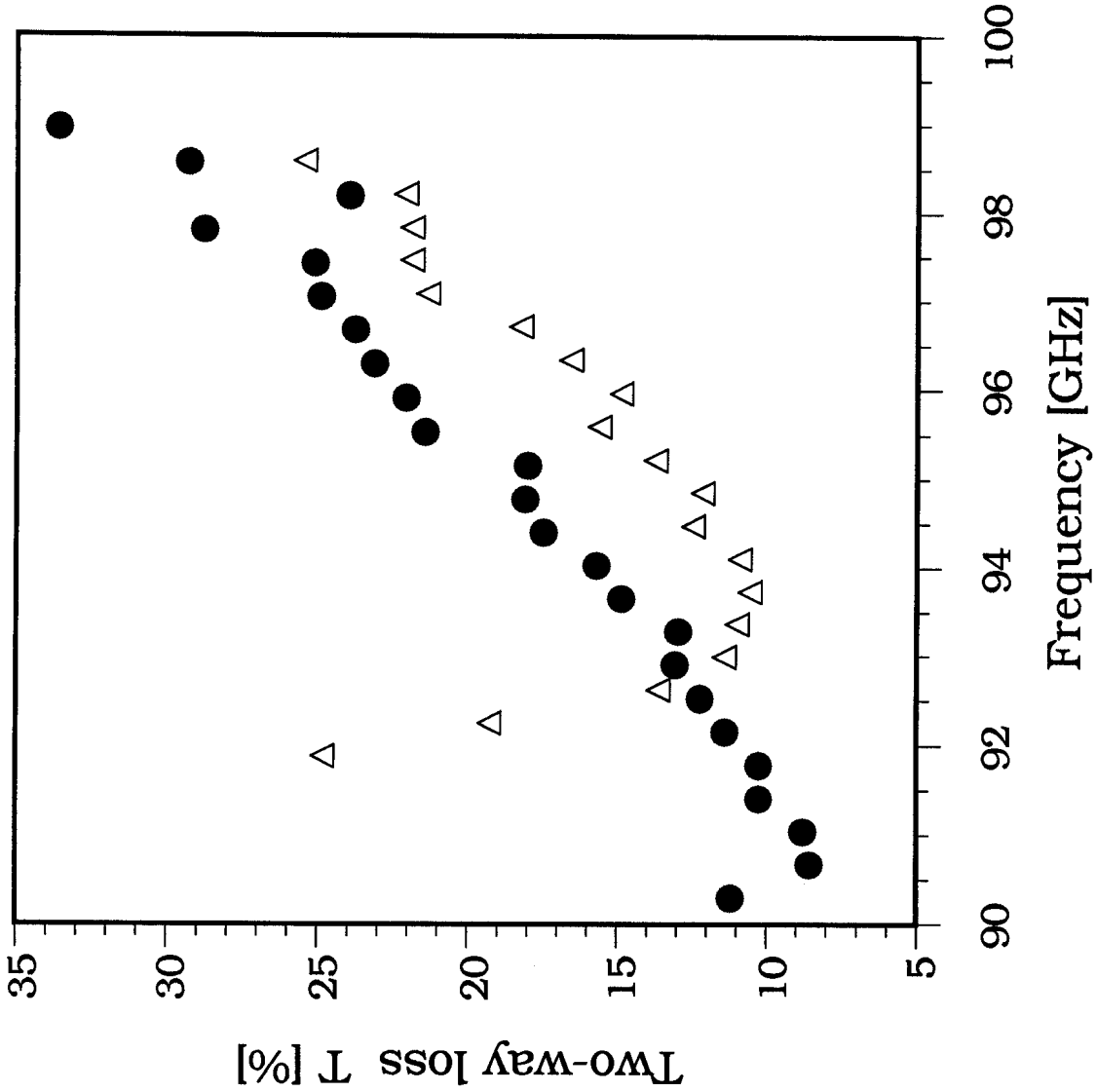

FIG. 16

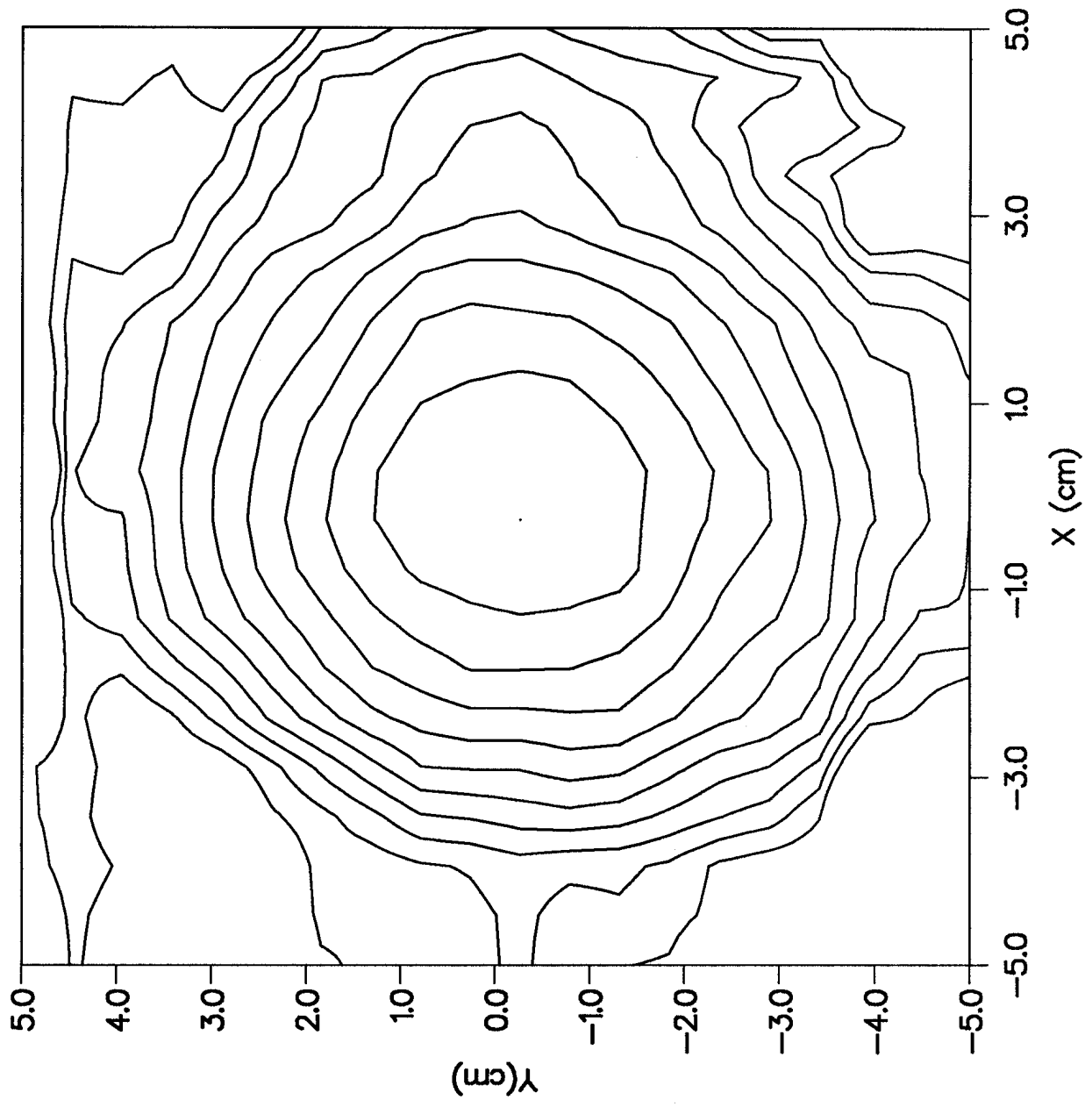

FIG. 17(a)

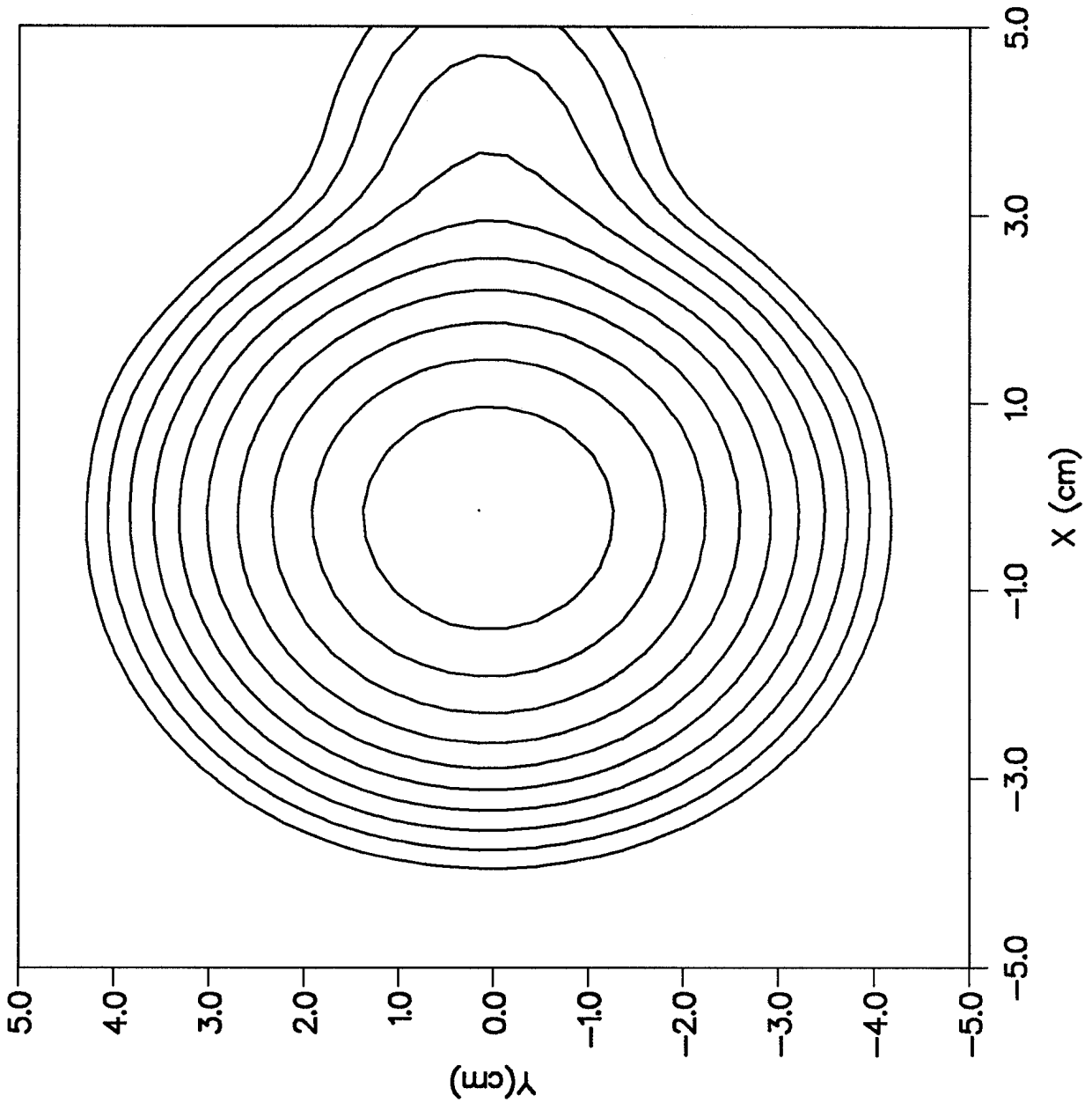

FIG. 17(b)

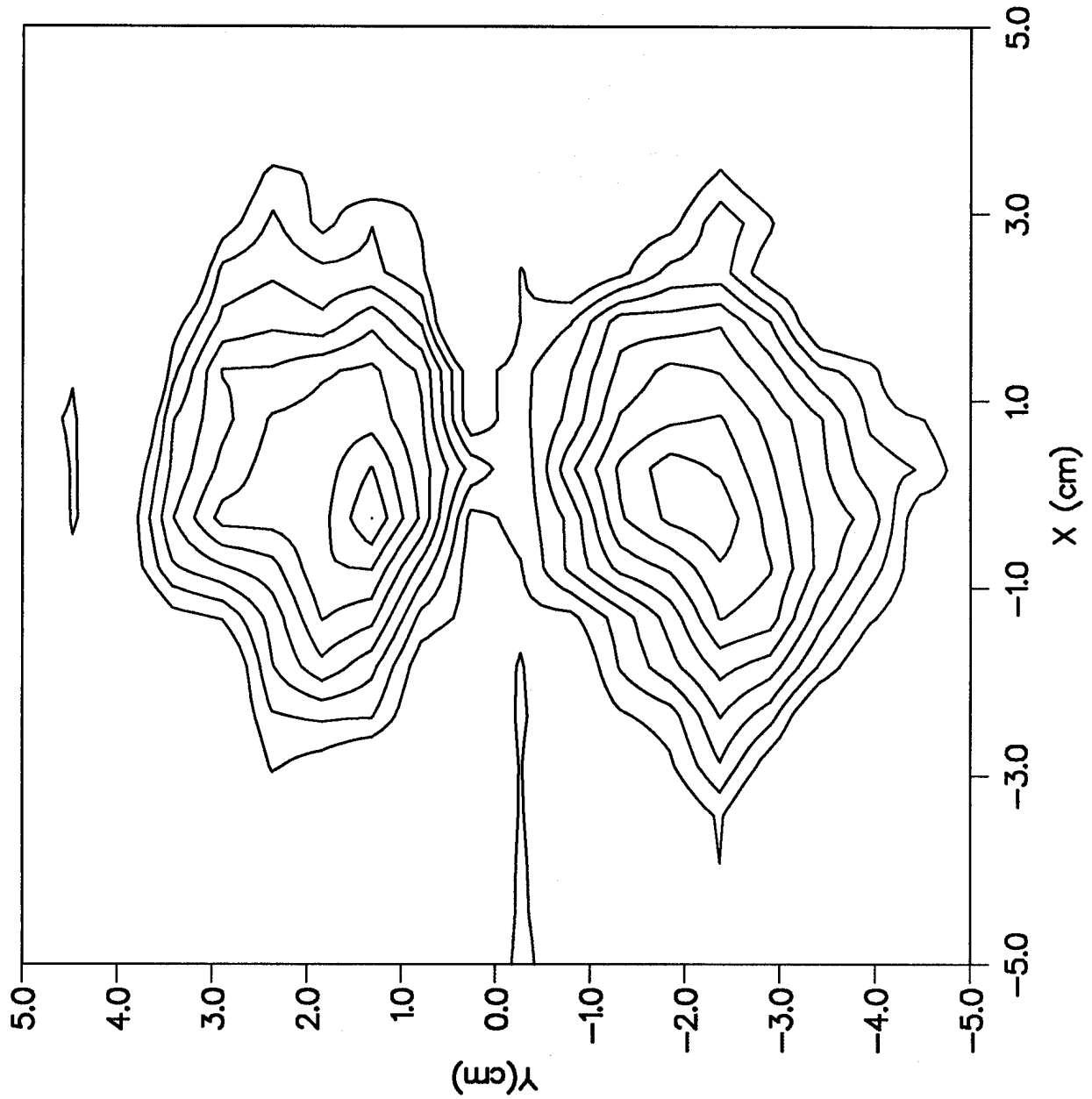

FIG. 18(a)

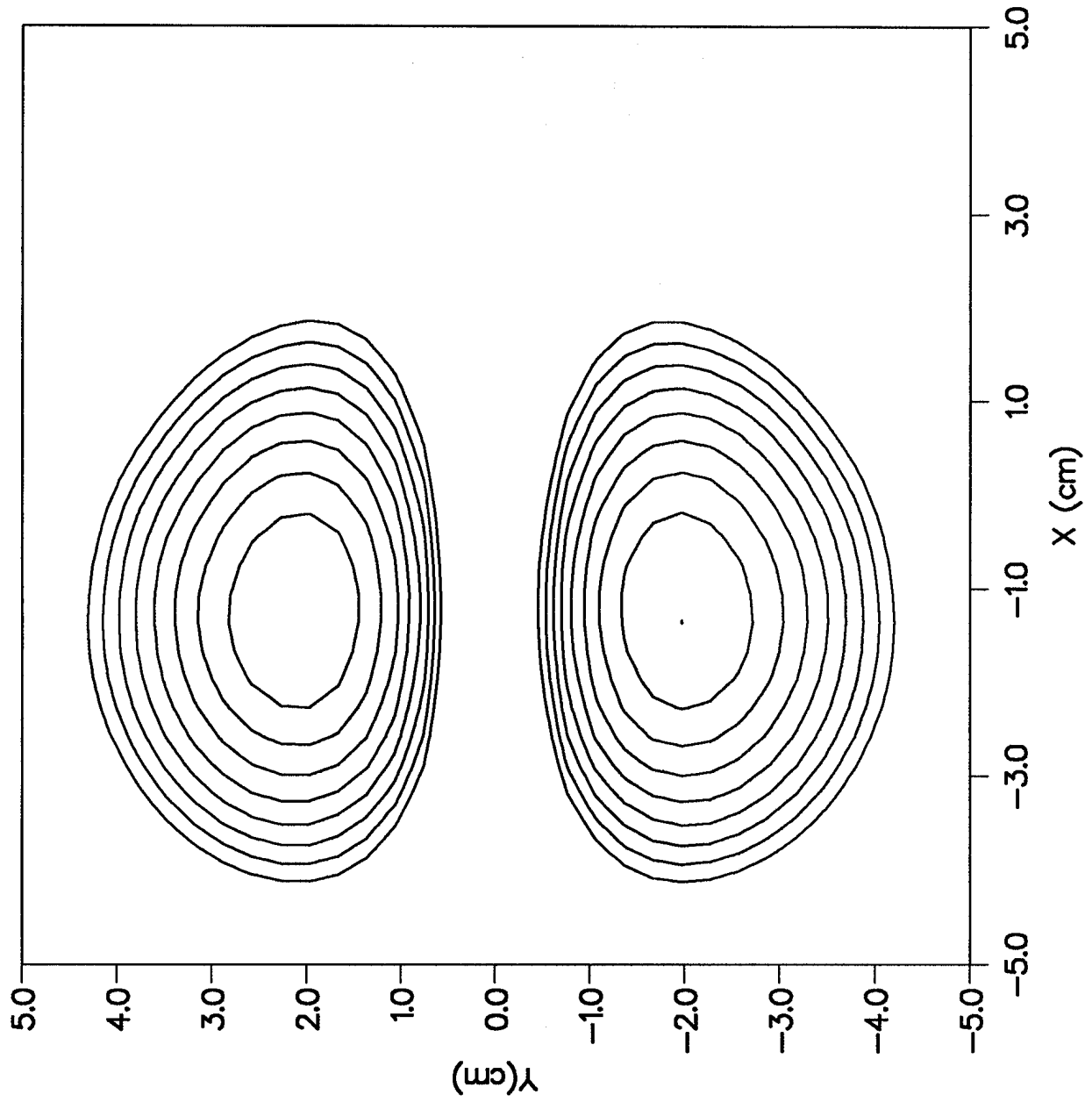

FIG. 18(b)

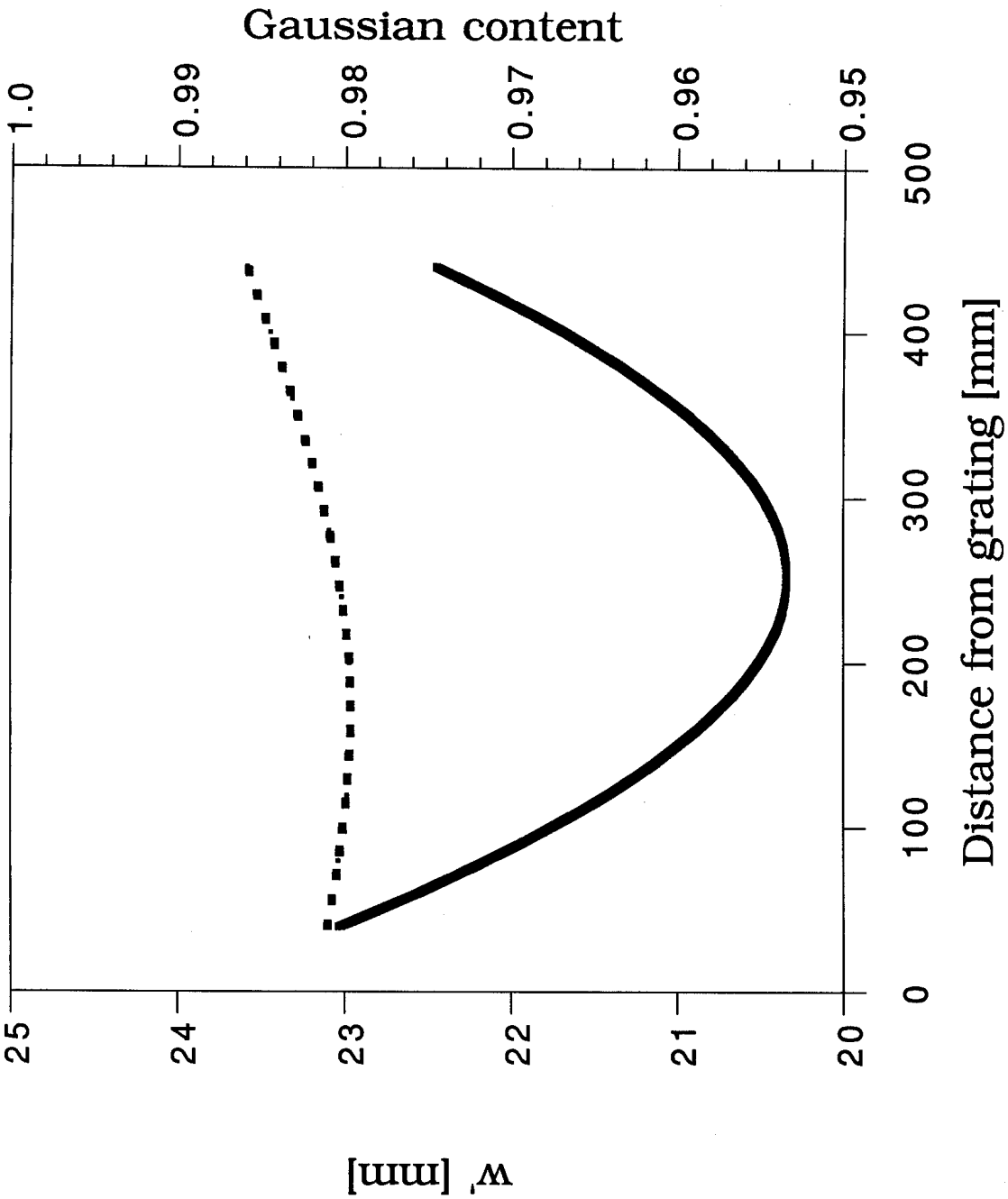
Gaussian content
1.0
0.99
0.98
0.97
0.96
0.95
25
24
23
22
21
20
0
100
200
300
400
500
Distance from grating [mm]
w' [mm]

FIG. 19